

## CRUCIAL PHYSICAL DEPENDENCIES OF THE CORE-COLLAPSE SUPERNOVA MECHANISM

ADAM BURROWS<sup>1</sup>, DAVID VARTANYAN<sup>1</sup>, JOSHUA C. DOLENCE<sup>2</sup>, M. AARON SKINNER<sup>3</sup>, DAVID RADICE<sup>1,4</sup>*Draft version November 18, 2016*

## ABSTRACT

We explore with self-consistent 2D FORNAX simulations the dependence of the outcome of collapse on many-body corrections to neutrino-nucleon cross sections, pre-collapse seed perturbations, and inelastic neutrino-electron and neutrino-nucleon scattering. We show here for the first time that modest many-body corrections to neutrino-nucleon scattering, well-motivated by physics, make explosions easier in models of core-collapse supernovae. In this sense, realistic many-body corrections could be important missing pieces of physics needed to ensure robust supernova explosions. In addition, we find that imposed seed perturbations, while not necessarily determinative of explosion, can facilitate it and shorten its post-bounce emergence time. We now find that all our multi-D models with realistic physics explode by the neutrino heating mechanism. Proximity to criticality amplifies the role of even small changes in the neutrino-matter couplings, and such changes can together add to produce dramatic effects. When close to the critical condition the cumulative result of a few small effects (including seeds) that individually have only modest consequence can convert an anemic into a robust explosion, or even a dud into a blast. Such sensitivity is not seen in one dimension and may explain the apparent heterogeneity in the outcomes of detailed simulations performed internationally. A natural conclusion is that the different groups collectively are closer to a realistic understanding of the mechanism of core-collapse supernovae than might have seemed apparent.

*Subject headings:* (stars:)supernovae; general

## 1. INTRODUCTION

A goal of core-collapse supernova theory is to explain the mechanism of explosion. It is an accepted truism of the field that a necessary condition for this is that complicated multi-dimensional simulation codes incorporating the requisite neutrino, nuclear, and gravitational physics reproduce such explosions robustly, yielding at the very least the requisite asymptotic energies, residual neutron star masses, and nucleosynthesis. A simple analytic explanation has not been forthcoming and, given the manifest complexities of the process, would not be deemed credible. It is thought that one litmus test of success would be such a demonstration for a non-rotating model between  $\sim 8$  and  $\sim 20 M_{\odot}$ , the progenitor ZAMS mass regime that must provide the lion's share of core-collapse supernova events.

However, to date the various groups engaged in such efforts around the world have failed to agree on the outcomes of the collapse of otherwise similar progenitor massive star cores. This is despite claims to have embedded the necessary physics and microphysics into the simulations. In fact, the numerical algorithms, resolutions, and input physics all differ, and even when the physics is deemed similar, the implementations and approximations surely differ. The ORNL group (Bruenn et al. 2013, 2016), with their CHIMERA code, uses multi-group flux-limited diffusion (MGFLD) neutrino trans-

port (Bruenn 1985), the VH-1 Newtonian hydrodynamics package, a monopole correction for general relativity (GR) (Marek et al. 2006), but multiple one-dimensional solves for multi-dimensional transport using the so-called “ray-by-ray+” approach (Buras et al. 2003; Burrows, Hayes, & Fryxell 1995). Such a dimensional reduction for the transport, particularly manifest in 2D, ignores lateral, non-radial radiative transport, which has been shown to be of quantitative (Ott et al. 2008; Brandt et al. 2011; Burrows 2013; Dolence, Burrows, & Zhang 2015; Sumiyoshi et al. 2015) and qualitative (Skinner, Burrows, & Dolence 2016) importance. To the point, Skinner et al. (2016) have shown that the ray-by-ray anomalies in the angular distribution of the radiation field and corresponding neutrino heating rates can reinforce the axial sloshing motions in 2D and push the shock into explosion<sup>5</sup>. Bruenn et al. (2013, 2016) find explosions in 2D (axially symmetry) for all the progenitors they studied (the 12-, 15-, 20-, and 25- $M_{\odot}$  models of Woosley & Heger 2007), but the models all explode at about the same post-bounce time ( $\sim 100$  milliseconds) and the shock radii never decrease in value. When performed in 3D for the 15- $M_{\odot}$  model of Woosley & Heger (2007), Lentz et al. (2015) obtain a weaker explosion delayed in its onset by an extra  $\sim 100$  milliseconds.

Müller et al. (2012ab), using the conformally-flat CoCoNuT hydrodynamics code in combination with the VERTEX transport solver and the ray-by-ray+ approach, find that models explode in 2D, but explode with lower energies and at post-bounce explosion times that differ significantly from those found by the ORNL group.

<sup>5</sup> However, the general absence in 3D of either an axial effect or the pronounced sloshing seen in 2D may be rendering 3D simulations performed with the ray-by-ray approach less problematic. This has yet to be tested.

<sup>1</sup> Department of Astrophysical Sciences, Princeton University, Princeton, NJ 08544; burrows@astro.princeton.edu; dvar-tany@princeton.edu; dradice@astro.princeton.edu

<sup>2</sup> CCS-2, Los Alamos National Laboratory, P.O. Box 1663 Los Alamos, NM 87545; jdolence@lanl.gov

<sup>3</sup> Livermore National Laboratory, 7000 East Ave., Livermore, CA 94550-9234; skinner15@llnl.gov

<sup>4</sup> Schmidt Fellow, Institute for Advanced Study, 1 Einstein Drive, Princeton, NJ 08540

In addition, their shock radii generally decrease from a peak occurring near a time  $\sim 200$  ms after bounce, before increasing just prior to explosion hundreds of milliseconds later (and all at different post-bounce times). Using the VERTEX-PROMETHEUS code, the Garching group obtained weak explosions in 2D for a  $11.2\text{-}M_{\odot}$  progenitor (Buras et al. 2006) and for a rotating  $15\text{-}M_{\odot}$  progenitor (Marek & Janka 2009), though the outcomes when proper correction is made for the corresponding mantle binding energies were not clear. More recently, the Garching group (Summa et al. 2016) obtained explosions in 2D for a broad range of Woosley & Heger (2007) progenitors from 11 to  $28\text{ }M_{\odot}$ , but these calculations as well did not comport with those of the ORNL group in the timescales and energies seen. The Garching group has also used for all their multi-D VERTEX supernova simulations a variant of the problematic ray-by-ray+ dimensionally-reduced transport approach.

However, Murphy, Dolence, & Burrows (2013) and Couch & Ott (2015), and originally Burrows, Hayes, & Fryxell (1995), highlight the importance of turbulent pressure behind the shock as an aid to explosion, but note that such a pressure is larger (artificially) in 2D than in 3D. Turbulent pressure is also (possibly) more anisotropic in 2D, favoring the radial stress component, further enhancing the prospects (again, artificially) for overcoming the accretion ram pressure. Hence, the current explosions in 2D may in part, or at times, be numerical artifacts.

Importantly, the recent VERTEX-PROMETHEUS calculations in 3D by the Garching group do not explode (Hanke et al. 2013; Tamborra et al. 2014), even though the corresponding 2D simulations did. Puzzled by this 2D/3D difference, Hanke et al. (2012) have speculated that the sloshing motion oftentimes associated in 2D with the SASI (standing accretion shock instability) may be crucial to explosion, though in 3D such a pronounced axial sloshing motion is rarely in evidence (Burrows et al. 2012). However, with slightly altered microphysics, in particular with a change in the axial-vector coupling constant ( $g_A$ ) due to a speculative enhanced effect on the nucleon spin of the strange quark, Melson et al. (2015) do obtain a weak explosion in 3D of the Woosley & Heger (2007)  $20\text{-}M_{\odot}$  in 3D. The difference in outcome is due to the consequent decrease in the neutrino-neutron neutral-current scattering cross section in the neutron-rich envelope of the protoneutron star bounded by the stalled shock and the resultant increase in the electron-neutrino luminosity and average energy that are instrumental in heating this envelope. However, the magnitude of the strangeness correction employed by Melson et al. may be larger than experiment allows (Ahmed et al. 2012). Furthermore, it is not at all clear that any among these currently published under-powered 3D explosions will actually succeed as an explosion after transversing the entire star and after the mass cut between ejecta and residual core is determined hydrodynamically.

The calculations of Burrows et al. (2006, 2007a) and Ott et al. (2008), using the VULCAN/2D code, and Dolence, Burrows, & Zhang (2015), using the CASTRO code (Zhang et al. (2011, 2013) employed multi-dimensional transport, and not ray-by-ray+, but in neither of these 2D studies did the authors see explosions by the neutrino mechanism. VULCAN/2D did not have

all the terms to order  $v/c$  in the transport, but CASTRO did, and the results were similar (Dolence, Burrows & Zhang 2015). Importantly, neither VULCAN/2D nor CASTRO made corrections for the effects of general relativity, and this could explain in part the different outcome. However, since other self-consistent calculations (summarized previously) that obtained explosions in 2D used the ray-by-ray scheme, while the VULCAN/2D and CASTRO studies did not, one is tempted to suggest that the ray-by-ray approach may in 2D be yielding qualitatively incorrect results.

Suwa et al. (2010) obtain an explosion in 2D of a  $13\text{-}M_{\odot}$  progenitor, while Takiwaki et al. (2012) obtain an explosion for an  $11.2\text{-}M_{\odot}$  progenitor in both 2D and 3D. Both these efforts, however, neglect  $\nu_{\mu}$  and  $\nu_{\tau}$  neutrinos, which constitute roughly 50% of the total neutrino losses after bounce, and use the IDSA (Liebendörfer et al. 2009) and ray-by-ray approximations for the transport. Suwa et al. (2010) and Nakamura et al. (2014) found that rotation aided explosion, mostly by rotationally expanding the size of the gain region and increasing the mass it contained. Iwakami, Nagakura, & Yamada (2014) and Takiwaki et al. (2016) highlight the rotational excitation of  $m = 1$  spiral-arm modes and find a role for non-axisymmetric rotational instabilities. Iwakami, Nagakura, & Yamada (2014) also used the IDSA and ray-by-ray transport approximations, and neglected “ $\nu_{\mu}$ ” neutrinos. Both Nakamura et al. (2014) and Takiwaki et al. (2016) observed equatorial explosions in the rapidly-rotating context. Recently, Janka et al. (2016) provided a preliminary look at a rapid-rotating 3D model that exploded. Earlier, Fryer & Heger (2000) used SPH for the hydrodynamics and a simplified gray scheme for the neutrino transport to explore the role of rapid rotation. Moreover, in all of these studies the initial rotation rate was not only high in the mantle, but was high in the core. Such rapid initial spins (periods of a few seconds) and final spins (periods of  $\sim 2\text{--}10$  milliseconds) seem not to be consistent with inferred pulsar spin periods at birth (crudely,  $\sim 300 \pm 200$  milliseconds; Emmering & Chevalier 1989; Faucher-Giguere & Kaspi 2006; Popov & Turolla 2012; Noutsos et al. 2013) and may be associated only with hypernovae (Burrows et al. 2007c) and/or gamma-ray bursts (MacFadyen & Woosley 1999).

In this paper, we explore, with self-consistent 2D FORNAX (§2) simulations, the dependence of the outcome of collapse (most notably whether the model explodes) on neutrino-nucleon scattering rates (via modifications of in-medium response corrections due to many-body effects), pre-collapse convective perturbations, inelastic neutrino-electron scattering, and inelastic neutrino-nucleon scattering. We also continue our study, started in Skinner et al. (2016), of the issues raised by the use of the ray-by-ray+ method. What we find is that when the protoneutron star bounded by a stalled shock is close to the critical condition for explosion (Burrows & Goshy 1993), as it easily can be in the turbulent multi-D context, the sensitivity to explosion of small changes in the physical inputs is amplified. The magnitude of such changes might be only  $\sim 20\%$ , but the result can be qualitatively different, in particular whether the model explodes. In the 1D (spherical) case, the core is not sensitive to comparable changes (“Mazurek’s Law”), but, as we demonstrate in this paper, in the multi-D turbulent

(and chaotic) context, small changes in the physics can have a qualitative effect on explodability. This may explain why the various groups around the world simulating core-collapse supernovae can witness very different outcomes, despite the fact that they ostensibly are incorporating almost the same microphysics and similar computational approaches. Small differences are amplified near criticality in this chaotic context. The availability of a new generation of fast, but accurate, simulation codes, such as FORNAX (§2), and significant supercomputer resources enables rapid multi-parameter investigations in the multi-dimensional (in particular 2D), multi-physics context. Such wide-ranging explorations reveal patterns not easily discerned when one (or only a few) simulations are the focus of a paper and its (or their) results solely are mined.

## 2. NUMERICAL METHOD AND COMPUTATIONAL SETUP

We have developed an entirely new multi-dimensional, multi-group radiation/hydrodynamic code, FORNAX, for the study of core-collapse supernovae (Skinner, Burrows, & Dolence 2016; Dolence, Burrows, & Skinner 2016)<sup>6</sup>. It employs spherical coordinates in one, two, and three spatial dimensions, solves the comoving-frame, multi-group, two-moment, velocity-dependent transport equations to  $O(v/c)$ , and uses the M1 tensor closure for the second and third moments of the radiation fields (Dubroca & Feugeas 1999; Vaytet et al. 2011). For this paper, we focus on two spatial dimensions (2D) and employ a spherical grid. Three species of neutrino ( $\nu_e$ ,  $\bar{\nu}_e$ , and “ $\nu_\mu$ ” [ $\nu_\mu$ ,  $\bar{\nu}_\mu$ ,  $\nu_\tau$ , and  $\bar{\nu}_\tau$  lumped together]) are followed using an explicit Godunov characteristic method applied to the radiation transport operators, but an implicit solver for the radiation source terms. In this way, the radiative transport and transfer are handled locally, without the need for a global solution on the entire mesh. This is also the recent approach taken by Just, Obergaulinger, & Janka (2015) and O’Connor & Couch (2015), though with some important differences. By addressing the transport operator with an explicit method, we significantly reduce the computational complexity and communication overhead of traditional multi-dimensional radiative transfer solutions by bypassing the need for global iterative solvers that have proven to be slow and/or problematic beyond  $\sim 10,000$  cores. Strong scaling of the transport solution in three dimensions using FORNAX is excellent beyond 100,000 cores on Cray architectures (Dolence, Burrows, & Skinner 2016). The light-crossing time of a zone generally sets the timestep, but since the speed of light and the speed of sound in the inner core are not far apart in the core-collapse problem after bounce, this numerical stability constraint on the timestep is similar to the CFL constraint of the explicit hydrodynamics. Radiation quantities are reconstructed with linear profiles, and the calculated edge states are used to determine fluxes via an HLLE solver. In the non-hyperbolic regime, the HLLE fluxes are corrected to reduce numerical diffusion (O’Connor & Ott 2013). The momentum and energy transfer between the radiation and the gas are operator-split from the transport and addressed implicitly.

The hydrodynamics in FORNAX is based on a directionally-unsplitted Godunov-type finite-volume

method. Fluxes at cell faces are computed with the fast and accurate HLLC approximate Riemann solver based on left and right states reconstructed from the underlying volume-averaged states. The reconstruction is accomplished via a novel algorithm we developed specifically for FORNAX that uses moments of the coordinates within each cell and the volume-averaged states to reconstruct TVD-limited parabolic profiles, while requiring one less “ghost cell” than the standard PPM approach. The profiles always respect the cells’ volume averages and, in smooth parts of the solution away from extrema, yield third-order accurate states on the faces. To eliminate the carbuncle and related odd-even coupling phenomenon, FORNAX specifically detects strong, grid-aligned shocks and employs in neighboring cells HLLE, rather than HLLC, fluxes that introduce a small amount of smoothing in the transverse direction.

Without gravity, the coupled set of radiation/hydrodynamic equations conserves energy and momentum to machine accuracy. With gravity, energy conservation is excellent before and after core bounce. However, as with all other supernova codes, at bounce the total energy as defined in integral form glitches by  $\gtrsim 10^{49}$  ergs (Dolence, Burrows, & Skinner 2016)<sup>7</sup>. This is due to the fact that the gravitational terms are handled in the momentum and energy equations as source terms and are not in conservative divergence form.

The code is written in a covariant/coordinate-independent fashion, with generalized connection coefficients, and so can employ any coordinate mapping. This facilitates the use of any logically-Cartesian coordinate system and, if necessary, the artful distribution of zones. In the interior, to alleviate Courant limits due to converging angular zones, the code can deresolve in angle with decreasing radius, conserving hydrodynamic and radiative fluxes in a manner similar to the method employed in AMR codes at refinement boundaries. Gravity is handled in 2D and 3D with a monopole or a multipole solver (Müller & Steimetz 1995). When using the latter, we generally set the maximum spherical harmonic order necessary equal to twelve. The monopole gravitational term is altered to accommodate approximate general-relativistic gravity (Marek et al. 2006), and we employ the metric terms,  $g_{rr}$  and  $g_{tt}$ , derived from this potential to incorporate general relativistic redshift effects in the neutrino transport equations (in the manner of Rampp & Janka 2002; see also Skinner et al. 2016). The appendix describes our approach to GR in more detail. In 2D, rotation and a third component of the velocity vector can be included in the hydrodynamics. We use the  $K = 220$  MeV Lattimer-Swesty equation of state (EOS) for all simulations presented in this paper (Lattimer & Swesty 1991).

For these simulations, we follow twenty energy ( $\varepsilon_\nu$ ) groups for each of the  $\nu_e$ ,  $\bar{\nu}_e$ , and  $\nu_\mu$  species. For the  $\nu_e$  types, the neutrino energy  $\varepsilon_\nu$  varies logarithmically from 1 MeV to 300 MeV, while it varies from 1 MeV to 100 MeV for the  $\bar{\nu}_e$ s and  $\nu_\mu$ s. We have performed calculations with forty energy groups and found little difference in the

<sup>6</sup> The appendix contains the equations solved.

<sup>7</sup> Most supernova codes jump in this quantity at this time by more than  $10^{50}$  ergs.

results. As stated earlier, spherical coordinates are used. The radial coordinate,  $r$ , runs from 0 to 10,000 kilometers (km) in 608 zones. The radial grid smoothly transitions from uniform spacing with  $\Delta r = 0.5$  km in the interior to logarithmic spacing, with a transition radius near  $\sim 100$  km. The polar angular grid spacing covers the full  $180^\circ$  and varies smoothly from  $\approx 0.95^\circ$  at the poles to  $\approx 0.65^\circ$  at the equator in 256 zones.

A comprehensive set of neutrino-matter interactions are followed in FORNAX, and these are described in Burrows, Reddy, & Thompson (2006). They include weak magnetism and recoil corrections to neutrino-nucleon scattering and absorption (Horowitz 2002); ion-ion-correlations, weak screening, and form-factor corrections for neutrino-nucleus scattering; and inelastic neutrino-electron scattering using the scheme of Thompson, Burrows, & Pinto (2003) and the relativistic formalism summarized in Reddy et al. (1999). Inelastic neutrino-nucleon scattering is also included using a modified version of the Thompson, Burrows, & Pinto (2003) approach (§4). Neutrino sources and sinks due to nucleon-nucleon bremsstrahlung and electron-positron annihilation are included, as described in Thompson, Burrows, & Horvath (2000).

We also include a many-body structure factor ( $S_A$ ) correction to the axial-vector term in the neutrino-nucleon scattering rate due to the neutrino response to nuclear matter at (low) densities below  $\sim 10^{13}$  g cm $^{-3}$ , derived by Horowitz et al. (2016) using a virial approach. A many-body correction to the vector term is not imposed, but is subdominant. However, many-body effects in the charged-current sector and on absorption may be comparable (Burrows & Sawyer 1999; Roberts et al. 2012; Fischer 2016), but have not yet been included. Horowitz et al. (2016) attach their fit to  $S_A$  to that of Burrows & Sawyer (1998) at higher densities. From the latter work, such effects are known to be important at higher densities and relevant to long-term (many seconds) protoneutron star cooling, but may also play an important role in the neutrino decoupling region and in the explosion mechanism.  $S_A$  is less than one by as much as tens of percent and generally results in perceptively higher neutrino luminosities and average energies in the early supernova phase for all neutrino species. The effect of  $S_A$  can be larger than the similar and corresponding effect of weak magnetism on the neutrino-nucleon scattering rate.

### 3. THE EFFECT OF MANY-BODY NEUTRINO RESPONSE CORRECTIONS TO NEUTRINO-NUCLEON SCATTERING

Melson et al. (2015) invoked a modification in the axial-vector coupling constant ( $g_A$ ) due to a possible strangeness contribution to the nucleon spin of  $g_A^s = -0.2$ . This results in an approximate decrease in the neutrino-nucleon scattering rate of  $\sim 20\%$  and in Melson et al. the consequence was an explosion in 3D, even though they did not witness an explosion in 3D when using their default microphysical suite. Curiously, without their strangeness correction, the same model exploded in 2D. However, the value of the correction,  $g_A^s$ , they employed in their 3D model is likely too large and  $g_A^s$  may be closer to zero (Ahmed et al. 2012).

Many-body corrections to neutral-current and charged-current neutrino-nucleon interactions have been

discussed in the past (Burrows & Sawyer 1998, 1999; Hannestad & Raffelt 1998; Reddy et al. 1999; Roberts et al. 2012) in the context of protoneutron stars and supernovae, and have been known to affect the neutrino-matter reaction rates. Burrows & Sawyer (1998) in particular suggested that many-body corrections to the axial-vector and vector structure factors for neutrino-nucleon scattering could be of a magnitude sufficient to be of relevance to the viability of the neutrino-driven mechanism of core-collapse supernovae, but did not provide a robust estimate of the magnitude of this diminution much below nuclear densities. Importantly, Horowitz et al. (2016) have recently generalized their virial expansion approach to the nuclear-matter equation of state to estimate the axial-vector structure factor ( $S_A$ ) of nuclear matter at lower densities ( $\geq 10^{11}$  g cm $^{-3}$ ), where it may have a bearing on the neutrino-driven mechanism.

The fit derived by Horowitz et al. (2016) to the structure factor applied to  $g_A^2$  translates into a decrease in the neutrino-nucleon scattering cross section in the crucial region at and deeper than the various neutrinospheres of  $\sim 5\%$  to  $\sim 35\%$ . This effect is a function of density, temperature, and electron fraction ( $Y_e$ ) and is comparable to, and can be larger than, the supposed strangeness correction invoked by Melson et al. (2015). Horowitz et al. (2016) state (without calculating) that the corresponding structure factor for the vector current is likely greater than one, but since the vector contribution to neutrino-nucleon scattering is small, this is likely to be subdominant. The upshot is a potentially important, and physically plausible, decrease in the neutrino-matter scattering rates that translates into an increase in the driving  $\nu_e$  and  $\bar{\nu}_e$  luminosities and average energies, thereby increasing the heating rate in the gain region. We show here for the first time that this augmentation, well-motivated by physics, makes explosions easier in multi-D (here 2D) models of the neutrino mechanism of core-collapse supernovae.

This many-body effect is mostly due to the increase in the  $\nu_\mu$  luminosity occasioned by the decrease in the associated  $\nu_\mu + n, p \rightarrow \nu_\mu + n, p$  scattering cross section for densities above  $\sim 10^{12}$  g cm $^{-3}$ ; this causes a further compression in the core. Such a compression, similar to the effect of GR, raises the temperatures near the  $\nu_e$  and  $\bar{\nu}_e$  neutrinospheres, thereby raising their associated luminosities and average emergent neutrino energies. These changes increase the neutrino-matter heating rates in the gain region and, hence, facilitate explosion. Since the super-allowed charged-current absorption reactions still dominate the  $\nu_e/\bar{\nu}_e$ -matter interaction rates, the direct effect of this structure factor correction to the axial-vector term in the neutrino-nucleon scattering rate on the  $\nu_e$  and  $\bar{\nu}_e$  luminosities is modest.

We note that the corresponding correction for charged-current interactions may be in the same direction (Fischer 2016; Burrows & Sawyer 1999, although see Roberts et al. 2012) and could also be important. The correction would be small at low densities in the gain region, but higher deeper inside, where the neutrinospheres reside. If the rates are suppressed, this could increase the  $\nu_e$  and  $\bar{\nu}_e$  luminosities, while simultaneously not decreasing the heating in the gain region and is not like a uniform cor-

rection at all radii. Such behavior, if it obtains, would be near optimal for aiding the explosion, and we will explore this correction to the charged-current interaction rates in subsequent work.

Figure 1 is the first in a series of figures we have generated for this paper depicting the time evolution of the mean shock radius with time after bounce of the 20- $M_{\odot}$  progenitor model of Woosley & Heger (2007). We choose the 20- $M_{\odot}$  model only for specificity. While the quantitative results differ for other progenitors, the qualitative results are similar. One of the central results that can be gleaned from such figures is the time of explosion. This quantity can help one gauge the relative role of the inputs in question. The focus of Figure 1 is on the effect of the inclusion of the many-body structure-factor correction. Similar figures corresponding to the roles inelastic scattering on nucleons (§4), perturbations (§5, and the ray-by-ray+ (§6) simplification are provided in subsequent sections and they collectively contain some of our core conclusions. Almost all models explode eventually. However, the time to explosion can vary significantly with inputs. While there are many combinatoric possibilities, we have settled on just a few pairwise comparisons to demonstrate the effects we see universally. Figure 2 depicts the post-bounce evolution of many of the same models performed in 1D. None of those 1D runs exploded, nor do any of our other 1D models with ZAMS masses greater than or equal to 12  $M_{\odot}$ . We employ the notation IES, INS, MB, pert, and rbrp to indicate “inelastic neutrino-electron,” “inelastic neutrino-nucleon,” “many-body,” “perturbations,” and “ray-by-ray+,” respectively. GR and the full suite of microphysics (Burrows, Reddy, & Thompson 2006) are always included and the models are non-rotating.

Figure 1 highlights the significant role the axial-vector structure factor correction of Horowitz et al. (2016) plays in the time of explosion. The thick black arrow connects two full-GR models, one with inelastic neutrino-electron and neutrino-nucleon scattering included with the full default suite of elastic scattering and absorption processes and the other adding the many-body correction on top of this. While the first model explodes, adding in the many-body correction decreases the post-bounce time to explosion by  $\sim 150$  milliseconds. In Figure 1, we also compare an IES-only and an IES\_MB model. Here, the effect of adding the many-body correction is larger.

The slight increase in the heating in the gain region due to the inclusion of inelastic neutrino-electron and neutrino-nucleon scattering is helpful, but the effect of the many-body correction is larger. Figure 3 compares the emergent neutrino luminosities (left panel) and root-mean-square (rms) neutrino energies (right) for these two models. The boosting in the  $\nu_{\mu}$  luminosity and rms energy is clearly manifest, as are the corresponding boosts in those quantities for the  $\nu_e$  and  $\bar{\nu}_e$  neutrinos. While one may have speculated that enhanced neutrino losses, particularly due to  $\nu_{\mu}$ s that are almost ineffectual in heating the shocked mantle, would have had a negative effect on explodability, the converse is true. Greater losses lead to a further compaction of the core with an increase in the matter temperatures near the  $\nu_e$  and  $\bar{\nu}_e$  neutrinospheres. The result is similar in effect to that of GR, whereby such core heating enhances the driving  $\nu_e$  and  $\bar{\nu}_e$  luminosities and the average neutrino energies, which in turn

enhance the heating power in the gain region. Since it is this power deposition that ultimately drives explosions, the net effect is quite supportive of explosion.

However, the actual magnitude and form of the correction to the axial-vector coupling term in the expression for the neutrino-nucleon scattering rate may be different from that derived by Horowitz et al. (2016) and this still needs to be verified. Moreover, the effects of similar many-body corrections to the absorption rates need to be incorporated, as do those for the vector coupling strengths. One prediction of the consequence of the structure-factor correction we have employed is the enhanced  $\nu_{\mu}$  luminosities and average energies seen in Figure 3. It is noteworthy that, as it stands, the effect on the outcome of core-collapse of many-body rate suppressions (Burrows & Sawyer 1998, 1999) might be large. If more careful analyses partially mute the magnitude of the effect we have highlighted here, the resultant explosion times might then populate the gap shown in Figure 1 between the the model with inelastic neutrino-electron and neutrino-nucleon scattering alone and that including the current Horowitz et al. (2016) correction. In addition, the  $\nu_{\mu}$  luminosity and neutrino energy boosts seen in Figure 3 might be more modest. This all remains to be determined.

#### 4. THE ROLE OF INELASTIC NEUTRINO-ELECTRON AND NEUTRINO-NUCLEON SCATTERING

Neutrino-electron scattering rates and cross sections are much smaller than those for neutrino-nucleon scattering, which themselves are smaller still than those for super-allowed charged-current reactions such as  $\nu_e + n \rightarrow p + e^{-}$ . For  $\varepsilon_{\nu} = 10$  MeV, this deficit is approximately two orders of magnitude. However, due to the small mass of the electron, the energy transfer to the matter during a “Compton-like” neutrino-electron scattering is on average quite large, while, due to the large mass of the nucleon, the corresponding average energy transfer during neutrino-nucleon scattering is rather small. Therefore, the large cross section for neutrino-nucleon scattering multiplied by the small associated energy transfer can be comparable to the product of the small neutrino-electron cross section with the large per-interaction energy transfer and depend upon temperature, density, and neutrino energy (Janka et al. 1996; Thompson, Burrows, & Horvath 2000). The upshot is that inelastic scattering off both electrons and nucleons can modify thermal profiles and heating rates exterior to the neutrinospheres and in the gain region and contribute to explosion by the neutrino heating mechanism. Moreover, Müller et al. (2012b) make the point that heating by  $\nu_{\mu}$ -nucleon inelastic energy transfer can boost the temperatures near the  $\nu_e$  and  $\bar{\nu}_e$  neutrinospheres and results in slightly higher  $\nu_e$  and  $\bar{\nu}_e$  energy luminosities, which in turn enhance heating behind the shock correspondingly. Our calculations corroborate this effect.

The detailed theory of the structure functions and redistribution kernels for such inelastic scattering, including the effects of final-state blocking and the thermal spectrum of the targets, can be found in Burrows, Reddy, & Thompson (2006), Reddy et al. (1999), Thompson, Burrows, & Pinto (2003), and Thompson, Burrows, & Horvath (2000). Pioneering work on inelastic scattering off electrons in the core-collapse context can be found in

Bruenn (1985) and Mezzacappa & Bruenn (1993). However, those latter papers were focussed on the downscattering effect due to inelastic  $\nu_e$ - $e^-$  scattering on the electron neutrinos produced during infall and the consequent decrease in the trapped lepton fraction. Since a larger trapped lepton fraction could help facilitate immediate post-bounce explosions (Burrows & Lattimer 1983), this quantity was more relevant when the prompt hydrodynamic supernova mechanism still seemed viable. However, with the emergence of the delayed, neutrino-driven mechanism (Bethe & Wilson 1985), and the conclusion that the prompt mechanism could not work due to catastrophic neutrino losses at and around shock breakout, the value of the trapped lepton fraction, and its precise value, receded in significance.

Nevertheless, heating behind the stalled shock due to inelastic energy transfer from neutrinos to both electrons and nucleons, or boosting the  $\nu_e$  and  $\bar{\nu}_e$  luminosities by  $\nu_\mu$  downscattering near their neutrinospheres (Müller et al. 2012b), may help achieve the critical condition for explosion, particularly when in concert with the inclusion of the in-medium neutrino response (Horowitz et al. 2016; §3) and the slightly net positive influence of GR. Heating by inelastic neutrino-electron scattering is still subdominant with respect to that due to charged-current  $\nu_e$  and  $\bar{\nu}_e$  absorption, and in 1D (spherical) simulations there is almost no hydrodynamic consequence of its inclusion (Thompson, Burrows, & Pinto 2003). The same can be said of inelastic neutrino-nucleon scattering (Janka et al. 1996; Burrows & Sawyer 1998, 1999; Thompson, Burrows, & Horvath 2000). However, in the realistic multi-D context of the core-collapse phenomenon, the cumulative effect of the addition of a few sub-dominant heating mechanisms, compression due to enhanced  $\nu_\mu$  neutrino losses and consequent  $\nu_e$  and  $\bar{\nu}_e$  neutrinosphere heating<sup>8</sup>, and greater proximity to the critical condition due to multi-D effects<sup>9</sup> amplifies the leverage of even small additions to the gain-region heating power over their effects individually and can convert an anemic explosion into a robust explosion, or even a dud into a blast. One recalls that the original delayed mechanism of Wilson required for explosion only a modest enhancement of  $\sim 25\%$  in the neutrino luminosity<sup>10</sup>.

For inelastic scattering off electrons of all neutrino species we use the formalism of Thompson, Burrows, & Pinto (2006), with the special-relativistic corrections in Reddy et al. (1999). For inelastic scattering and energy redistribution of  $\nu_e$ s and  $\bar{\nu}_e$ s off nucleons, we use the formalism of Burrows & Sawyer (1998), but for inelastic scattering of  $\nu_\mu$  off nucleons we use an approximate approach advocated by Müller & Janka (2015). However, from the work of Thompson, Burrows, & Horvath (2000) and Tubbs (1979), we find that the crossover energy between upscattering and downscattering is nearer

$6k_B T$  (not  $3k_B T$ , as in Müller & Janka), where  $k_B$  is Boltzmann’s constant and  $T$  is the temperature, around densities of  $\sim 10^{11}$  g cm<sup>-3</sup> to  $\sim 10^{13}$  g cm<sup>-3</sup> and so our approximate redistribution rate for  $\nu_\mu$ s is proportional to  $\kappa_{scat}(\varepsilon_\mu - 6k_B T)/m_n c^2$ , where  $\kappa_{scat}$  is the  $\nu_\mu$  scattering opacity and  $m_n$  is the neutron mass.

Figure 4 is the same as Figure 1, but highlights the comparison between two different models, one with inelastic scattering off electrons and the other with inelastic scattering off both electrons and nucleons. One sees that the time to explosion of this 20-M<sub>⊙</sub> model is clearly shortened by inelastic neutrino-nucleon scattering effects. Figure 5 compares the neutrino luminosity evolution for these two models. Inelastic scattering off nucleons lowers the  $\nu_\mu$  luminosity, while the corresponding quantities for the  $\nu_e$  and  $\bar{\nu}_e$  are slightly increased. The latter responses explain the positive effect on explodability of the inclusion of inelastic scattering off nucleons. We emphasize that the direct effect of such inelasticity is in the core, and that the effect in the shocked mantle is indirect.

Including only inelastic neutrino-electron scattering, our 20-M<sub>⊙</sub> model explodes, but late (after  $\sim 0.9$  seconds). Including both inelastic neutrino-electron scattering and inelastic neutrino-nucleon scattering, the 20-M<sub>⊙</sub> model explodes significantly earlier. However, as shown on Figure 8 in §7 below, without the many-body correction, our 12- and 15-M<sub>⊙</sub> models do not explode within 1.0 seconds of bounce. These models explode only when the many-body structure factor decrease in the scattering rates is accounted for (and in fact even without incorporating neutrino-nucleon inelasticity). This emphasizes both the important roles of many-body effects and (perhaps) perturbations (§5) in igniting those “lighter” stars, and that compactness ratio (§8), for which the lighter models should have an advantage, is not necessarily a good measure of explodability.

## 5. A ROLE FOR PROGENITOR PERTURBATIONS

Performing the last stages of stellar evolution before collapse hydrodynamically in 2D and 3D has been shown to alter, perhaps in significant ways, the compositional, entropy, and density profiles of the core (Meakin et al. 2011; Couch et al. 2015; Chatzopoulos et al. 2016; Müller et al. 2016; Abdikamalov et al. 2016), and it has long been known that progenitor density profiles have an impact on the outcome of collapse. This is implicit in the critical curve analysis of Burrows & Goshy (1993), where  $\dot{M}$  and the accretion ram pressure play central roles. It is also a factor in discussions of the compactness parameter (O’Connor & Ott 2011) and its extensions (Ertl et al. 2015). In this vein, one notes that two groups (Kitaura et al. 2006; Burrows et al. 2007b) have already demonstrated that the 8.8-M<sub>⊙</sub> “electron-capture” supernova progenitor of Nomoto & Hashimoto (1988), with its extremely steep density ledge, can explode in 1D by the neutrino-driven wind mechanism, though the explosion energy is low ( $\sim 10^{50}$  ergs). Determining how progenitors derived using multi-D stellar evolution differ from those generated with 1D codes and mixing-length theory is an exciting topic to explore.

However, when spherical supernova models are wanting, the initial perturbation spectrum in the progenitor’s convective silicon and oxygen zones will certainly affect

<sup>8</sup> as in neutrino-electron scattering and many-body scattering rate suppression

<sup>9</sup> Examples include the enhancement of the stress behind the shock due to turbulent pressure (Burrows, Hayes, & Fryxell 1995; Murphy, Dolence, & Burrows 2013; Janka 2012; Burrows 2013) and the modest increase in the dwell time in the gain region of the post-shock matter (Murphy & Burrows 2008; Dolence et al. 2013)

<sup>10</sup> In that case, it was due to “neutron-finger convection,” subsequently later shown not to occur (Bruenn & Dineva 1996; Dessart et al. 2006).

the timescales for the generation of turbulence behind the stalled shock and may be a factor in the onset of explosion (Couch & Ott 2013; Müller & Janka 2015; Couch et al. 2015; Abdikamalov et al. 2016). Specifically, the magnitude, character, and spectra of seed perturbations will affect how quickly turbulence reaches the non-linear regime and, perhaps, whether turbulence grows to non-linearity at all during the finite time the accretors are in the unstable gain region.

Therefore, introducing physically-motivated seed perturbations that originate from and reflect the three-dimensional character of the convective core of an actual massive star at its terminal stage of evolution is a topic of some interest. However, most calculations done to date do not start with true 3D convective structures, but with 1D models from the literature, and impose either ad hoc perturbations in density or velocity randomly at the grid level or allow grid asphericities (such as obtain when using a Cartesian grid) or truncation errors to act as seeds. Neither of these approaches is physical, and the resulting initial perturbation spectra lead to early growth rates in the linear regime that reflect not the multi-D progenitor perturbation structure, but the numerical development of convenient artificial power spectra. This will affect how quickly turbulence reaches the non-linear regime and, perhaps, whether turbulence grows to non-linearity at all during the finite time the accretors are in the unstable gain region. In addition, this may have a bearing on the post-bounce delay to a turbulence-aided explosion, with the consequent effect on the time and energy of that explosion.

Therefore, the seed perturbations that arise during oxygen and silicon burning prior to collapse might be key inputs into core-collapse supernova theory, and Couch & Ott (2013), Müller & Janka (2015), Couch et al. (2015), and Müller (2016) have begun to explore this. However, mixing-length theory, though inadequate as a comprehensive theory, still provides a measure of the magnitude of velocity perturbations at the onset of collapse (Müller et al. 2016), and they are only a few hundred to  $\sim 500$  km s $^{-1}$ , with Mach numbers bounded by  $\sim 0.08$  (Woosley & Heger 2007). This is not large.

In this section, we provide a glimpse at the possible relative role of significant perturbations on the timing and character of explosion in light of the other physics. To this end, we employ the methodology of Müller & Janka (2015). These authors impose a vector velocity perturbation map on their progenitor that is more realistic than many past approaches and renders a perturbation field that is independent of grid resolution. This (surprisingly) was rarely attempted in the past and provides a specific context for future comparison. We set the maximum perturbation speed on the grid to 1000 km s $^{-1}$ , which as indicated earlier may be near or beyond the expected upper end of the range, a spherical harmonic index  $\ell$  of 2, and a radial “quantum number”  $n$  of 5. Both  $\ell$  and  $n$  are parameters in the Müller & Janka (2015) formulation. With this parameter set, we simulate in 2D the self-consistent multi-group evolution of a 20- $M_{\odot}$  progenitor and compare the result to a default model for which the initial perturbations are much smaller and arose numerically from grid noise.

Figure 6 provides a comparison of two 20- $M_{\odot}$  mod-

els: one with and one without the initial perturbation structure discussed above. This pair of models incorporates GR and inelastic neutrino-electron scattering, but neither the many-body correction nor inelastic neutrino-nucleon scattering. However, on Figure 6 we also include a comparison of two other models: one with GR and inelastic scattering off both electrons and nucleons and the other also with the same imposed perturbations. In Figure 6, comparison of the first pair of models demonstrates that when the baseline model includes only the small effect of inelastic neutrino-electron scattering, the effect of large perturbations on top of that baseline model is quite positive. When inelastic scattering off both electrons and nucleons is included, perturbations have even more leverage. The result in both cases is a decrease in explosion time of many hundreds of milliseconds. Providing the unstable flow in the gain region seed perturbations of sufficient magnitude ensures growth to fully non-linear turbulence, with the associated stress, during the finite-time traversal of the accreted matter through the crucial gain region. We conclude that imposed progenitor perturbations, while not determinative of explosion, can in principle facilitate it and shorten its post-bounce emergence time. When things are marginal, seed perturbations may make a difference. However, we also find that models that already explode robustly and early are not much aided by the imposition of seed perturbations in the initial models.

We note that the initial perturbations we imposed have an amplitude that is somewhat larger than expected (Müller et al. 2016) and that their character is still rather artificial. The magnitude of the initial perturbations may well be lower, but their character and magnitude will certainly vary from progenitor to progenitor. Models with weaker initial seed perturbations may well populate the wide gap seen in Figure 6. Therefore, a much more thorough study with 3D progenitors and 3D collapse models is called for. Be that as it may, none of the 2D explosion models we simulated that included all the microphysics, including the many-body correction and inelasticity, were enabled by such physically-motivated progenitor perturbations. They were, however, marginally facilitated.

## 6. RAY-BY-RAY+ ANOMALIES

As stated earlier, and as shown by Skinner et al. (2016), the ray-by-ray+ approach to neutrino transport, whereby multi-D transport is replaced by multiple 1D transport calculations with corrections for matter advection, but not lateral transport, can introduce systematic errors in the heating rates along the poles in axisymmetric 2D simulations. Such enhancements, when in proximity to criticality, may be producing explosions artificially. At the very least, the time to explosion is artificially shortened, perhaps significantly. Since there is little or no accumulation of explosion energy prior to global instability (Burrows, Hayes, & Fryxell 1995),<sup>11</sup> an earlier explosion may make more of the emitted neutrinos available for explosive driving.

Figure 7 highlights comparisons of two pairs of GR models, one pair with inelastic neutrino-electron scattering and the other pair with inelastic scattering off both

<sup>11</sup> Only those neutrinos emitted after the onset of the explosion contribute to the asymptotic explosion energy.

electrons and nucleons. Each set contrasts the results with the full multi-D transport capabilities of FORNAX and the corresponding ray-by-ray+ method. The ray-by-ray+ models explode as much as  $\sim 500$  and  $\sim 200$  milliseconds, respectively, earlier. Ray-by-ray+ models that also include the many-body structure-factor correction and inelasticity on both electrons and nucleons explode even earlier, but the additional shift in explosion time is not as great. In fact, the effect of using the ray-by-ray+ transport approach, but without the many-body correction, is similar to the effect of the many-body correction when using more realistic 2D transport. One is left to speculate whether 2D simulations in the literature that employ ray-by-ray+, but don't include our many-body suppression term, would indeed explode if they used more realistic transport. This is all the more relevant in 3D, given that extant published models that do explode in 2D have more difficulty exploding in 3D, a context in which it is not clear that the ray-by-ray+ method introduces as great an artifact as in 2D. It is true that the turbulent pressure spectra in 2D and 3D are different, with the turbulent cascade in 2D resulting in enhanced stresses on larger scales, and that the turbulent-stress boost to explosability may be smaller in 3D. This could also be a factor in the more anemic outcomes in published 3D models. Nevertheless, it may be that the more problematic nature of published 3D models vis-à-vis 2D models is a consequence of some combination of the use of ray-by-ray+, the reduced turbulent stress in 3D, and the lack of proper many-body suppression factors in those models. Hence, we suggest that the inclusion of many-body terms, whose effect we study in this paper (§3), can compensate for the (likely) smaller turbulent stress in 3D and the negative, but physical, effect of switching to real multi-D transport. In this sense, structure factor corrections could be a missing pieces of physics needed for robust supernova explosions in 3D. Of course, this will need to be tested, but our current results in this regard are quite encouraging.

## 7. A BENCHMARK SET OF TWO-DIMENSIONAL EXPLOSION SIMULATIONS

We now provide the salient results concerning our benchmark models for the 12-, 15-, 20-, and 25- $M_{\odot}$  progenitor models of Woosley & Heger (2007). We defer a much more extensive discussion on these and other models to a later paper (Vartanyan et al. 2017). These models include GR, the detailed microphysical neutrino-matter interaction suite of Burrows, Reddy, & Thompson (2006), the LS220 EOS, inelastic scattering on both electrons and nucleons, the many-body axial-vector structure factor correction to neutrino-nucleon scattering of Horowitz et al. (2016), and the full multi-D transport approach of FORNAX. All the models explode quite robustly. However, the perturbations arise from the dendritic grid and truncation error at machine level. Had we imposed further initial perturbations, the models would likely have exploded slightly earlier.

Figure 8 depicts the mean shock radii versus time after bounce for our model set. For comparison, we include the corresponding models without the many-body correction. We note the large difference in the time to explosion between our two model sets, with and without the many-body correction. Figure 9 compares the mean

shock radii versus post-bounce time of the Summa et al. (2016) 2D models with our calculations for the same progenitors with ostensibly the same physics inputs, but using the same ray-by-ray+ transport method they employ. Note that the many-body factor is not included. This figure also depicts the corresponding behavior for the Bruenn et al. (2016) 2D models and that of the Lentz et al. (2015) 15- $M_{\odot}$  model (“Series C”). There was no attempt a priori to reproduce the Summa et al. (2016) results, yet Figure 9 suggests that we have captured some of the essential elements of their simulations, although our earlier mean shock radii are as much as 30–50 km larger. The progenitor order of explosion and the post-bounce times to explosion seem to correspond rather well, given that, as we have shown, small differences in numerical approach, resolutions, and implementation of microphysics can result in significant variation in explosion time. The exceptions are the 12- $M_{\odot}$  and 15- $M_{\odot}$  progenitors, for which the baseline IES\_INS models do not explode within 1.0 second of bounce. We note that those models that explode at late times are always more susceptible to the smallest changes in the physical inputs, so the implied difference between our ray-by-ray+ 12- $M_{\odot}$  model and that of Summa et al. (2016) could otherwise be explained by very slight differences in inputs, methodology, and/or resolution. Be that as it may, the large differences in explosion time between the published 2D models of Bruenn et al. (2016) and Summa et al. (2016) remain unexplained. Interestingly, the 15- $M_{\odot}$  2D model of Lentz et al. (2015) corresponds quite well with our benchmark 15- $M_{\odot}$  model with the new many-body correction included, even though the same correction is not known to have been included in that work.

The so-called “diagnostic” explosion energies ( $E_{\text{diag}}$ ) versus time after bounce for each of these models are given in Figure 10, where  $E_{\text{diag}}$  is defined as the sum of the kinetic, internal, and gravitational energies of ejected matter with positive specific energy. We also include the recombination energy and the total energy of the matter exterior to the shock out to the 10,000-km boundary of our computational domain. The envelope binding energy of the progenitor exterior to 10,000 km will need to be overcome (if that matter is ultimately ejected), after the total deposited neutrino energy is asymptotically reached and the mass cut is completely determined. These 10,000-km envelope binding energies are  $\sim 0.069$ ,  $\sim 0.2$ ,  $\sim 0.49$ , and  $\sim 0.89$  Bethes ( $1 \text{ Bethe} \equiv 10^{51} \text{ erg}$ ) for the 12-, 15-, 20-, and 25- $M_{\odot}$  progenitors, respectively. Figure 11 plots the envelope binding energies for ultimate baryon mass cuts of 1.4, 1.5, and 1.6  $M_{\odot}$  for the Woosley & Heger (2007) progenitor models and gives an additional sense of the magnitude of the envelope binding energy to be overcome if a supernova is to emerge and leave behind a neutron star of the associated baryon mass. For stars less massive than 25  $M_{\odot}$ , this quantity generally increases rather quickly with ZAMS mass, if not completely monotonically, from  $\sim 0.1$  Bethe (at 12  $M_{\odot}$ ) to  $\sim 1.0$  Bethe. The envelope binding energy is significantly smaller below 12  $M_{\odot}$ . The large hump around  $\sim 40 M_{\odot}$  speaks volumes about the capacity of such progenitor models to explode with a neutron star residue. Since our explosion calculations were generally carried out to  $\sim 1.0$  second after bounce, the explosion energies of our benchmark models are still accumulating



at a significant rate at the end of our simulations.

As Figure 10 shows, at the termination of our simulations, the diagnostic energies of explosion (missing only the binding energy exterior to 10,000 km) are  $\sim 0.15$ ,  $\sim 0.35$ ,  $\sim 0.55$ , and  $\sim 0.6$  Bethes for the 12-, 15-, 20-, and 25- $M_{\odot}$  progenitors, respectively, while for the 20- and 25- $M_{\odot}$  progenitor models after about one second and without the many-body correction they are  $\sim 0.43$  and  $\sim 0.4$  Bethes, respectively. Without this correction, our 12- and 15- $M_{\odot}$  progenitor models do not explode within one second of bounce. For all progenitors except the 25- $M_{\odot}$  model, the benchmark diagnostic energies exceed the envelope binding energies by the end of the simulations. Moreover, all explosion energies are still accumulating at the (arbitrary) end of our runs.

We note that many of our benchmark 2D models explode asymmetrically (Vartanyan et al. 2017, in preparation). During the first  $\sim 0.5$  seconds into explosion, one hemisphere continues to experience accretion and contributes little to our estimate of the diagnostic explosion energy. This could be an artifact of the ring structure in axisymmetric 2D simulations and is not expected in 3D simulations of the same models (Dolence et al. 2013). However, continued accretion maintains higher driving luminosities, so whether we will actually realize this boost in the 3D models is not at all clear. Nevertheless, we speculate that our diagnostic explosion energies in 3D could be as much as a factor of two larger at the same phase of explosive evolution. We will explore this hypothesis in future work.

It has been suggested (Chugai & Utrobin 2014) that the explosion energy may be correlated with ZAMS mass, although the measured core-collapse supernova energies have yet to be pinned down. Though we have not carried our calculations out to the many seconds after bounce necessary to determine asymptotic explosion energies (Müller 2016), the set of diagnostic and envelope binding energies we witness suggests that total supernova energies may have a peak and are unlikely to be monotonic with ZAMS mass out to the larger masses.

For all exploding models, a secondary shock emerges at late times and catches up to the primary shock; this is the proto-neutron star wind (Burrows, Hayes, & Fryxell 1995). The maximum entropies of the ejecta at the end of our simulations are generally  $\sim 50$ – $60$ . For our benchmark 12, 15, 20, and 25  $M_{\odot}$  progenitor models, the baryon masses of the neutron stars left behind are 1.50, 1.70, 1.92, and 1.92  $M_{\odot}$ , respectively. These matters will be further explored in Vartanyan et al. (2017).

## 8. COMPACTNESS

Finally, we conclude that the compactness parameter (O’Connor & Ott 2011, 2013), defined at bounce for a given mass interior ( $M$ ) at a given radius ( $R$ ) as  $\xi \equiv M/M_{\odot}(1000\text{km}/R)$ , although it is one measure of the important density structure of the progenitor, is not necessarily predictive of explosion, at least during the first second after bounce. We find that, depending upon the neutrino physics employed, the temporal order in which models with different compactness parameters explode after bounce varies. Though the compactness parameter is large for the 25- $M_{\odot}$  model and small for the 12- $M_{\odot}$ , we found that the former can be more explodable than the latter when not including the many-body

correction. One might have thought that if compactness were the sole predictor the details of the neutrino-matter interaction would have mattered little in this regard. However, we see that the time to explosion does not necessarily correlate well with compactness. Models with dense envelopes have larger accretion and total neutrino luminosities after bounce, and it is these luminosities that drive explosion. In addition, models with dense envelopes and higher compactness have a greater optical depth to neutrinos in the gain region. Since the neutrino power deposition goes approximately as the product of this depth and the luminosities, high-compactness progenitors have an advantage. Therefore, it is feasible that more massive models might be more explosive, and this trend has been seen by other modelers (Summa et al. 2016; Bruenn et al. 2016). In fact, in the Summa et al. and Bruenn et al. papers for the Woosley & Heger (2007) models, the post-bounce explosion times increase in the sequence 20, 25, 15, and 12  $M_{\odot}$ , which is clearly not monotonic with compactness. Moreover, when the many-body term is dropped and seed perturbations are not imposed, our 12- $M_{\odot}$  models do not explode even after 1.0 seconds. This behavior is the reverse of what might be expected if low compactness signaled greater explodability.

A critical issue is whether these more massive models with shallower density profiles that explode early can maintain explosion during the traversal of the shock through the outer stellar mantle. The binding energy penalty of the outer envelope generally increases with progenitor mass and might be too steep a price to pay during subsequent evolution for those more massive cores that explode earlier (when they do, such as our 20- $M_{\odot}$  and 25- $M_{\odot}$  runs) and more energetically. As previously stated, for most of the relevant mass function, the envelope binding energy exterior to a given interior mass is an increasing function of progenitor mass. It is this “barrier” that may set the limit to the range of massive stars that can explode and leave behind neutron stars, although it cannot be excluded that the progenitor mass range that yields neutron stars, and not black holes, may be discontinuous (Sukhbold et al. 2016). Figure 12 depicts the close correspondence between the compactness and the envelope binding energy exterior to a baryonic mass cut of 1.5  $M_{\odot}$ . Therefore, we contend that whatever significance there may be to the compactness parameter is likely due to its correspondence with the binding energy of the outer envelope exterior to a given mass cut and that compactness need not correlate with the apparent explodability during the first second after core bounce. Importantly, the ultimate outcome will depend upon the progress of the shock at post-bounce times that generally exceed those to which most core-collapse simulations currently go.

## 9. CONCLUSIONS

In this paper, we have generated and explored detailed 2D (axisymmetric) GR models of core-collapse supernovae using the new code FORNAX, treating all the relevant physics to determine the dependence of the mechanism of explosion and its timing on the physical and numerical inputs and assumptions. These include inelastic neutrino-electron and neutrino-nucleon scattering, many-body/structure-factor corrections to the neutrino-

nucleon scattering rates, and physically-motivated initial perturbations. We have also reexamined in brief the effect of using the ray-by-ray+ simplification to neutrino transport. We found that much of the wide variation between the results, in particular the time to explosion and explosion energies, obtained by different groups around the world simulating stellar collapse (as well as whether the core explodes at all) might be explained by slight variations at the  $\sim 10\text{--}30\%$  level in the microphysical inputs when the models are near the critical condition for explosion. In the process, we gauged the relative importance of otherwise sub-dominant neutrino physics processes to the outcome of collapse. Proximity to criticality amplifies the dependence upon small changes in the neutrino sector that translate into slight, but crucial, changes in the emergent luminosities and average neutrino energies and the consequent post-shock heating rates; such sensitivity is not manifest in 1D simulations for which the core is (most often) far from explosive.

Thus, “Mazurek’s Law” of severe feedback under variations in neutrino cross sections and rates is overturned due to the proximity to instability possible in the realistic multi-D turbulent context. While alterations in the neutrino coupling rates have little effect in 1D, in multi-D the hydrodynamic response to even small changes and/or corrections to neutrino interaction rates can be more substantial due to greater proximity to the critical curve. This is one of the theses and motivating factors of this work.

The upshot is that small variations between the methods, microphysics, and resolutions used by groups who ostensibly are incorporating the “same” inputs translates naturally into post-bounce explosion time differences that can range by many hundreds of milliseconds, and in some cases can turn a dud into an explosion (or vice versa). We suggest that this thereby explains in large measure the apparent heterogeneity in the outcomes of detailed simulations performed internationally. A natural conclusion is that, viewed correctly, the different groups are collectively closer to a realistic understanding of the neutrino-driven mechanism of supernova explosion than might have seemed apparent and that a push to rationalize approaches and understand microphysical details in the neutrino-matter interaction sector and the nuclear equation of state could bring a resolution to the decades-long quest for a predictive model of core-collapse supernova explosions.

Importantly, we have found that many-body corrections to neutrino-matter scattering rates, even at sub-nuclear densities, can have as large an effect as, or even a larger effect than, general relativity, progenitor perturbations, or inelastic neutrino-electron and neutrino-nucleon scattering. The enhancement effects brought on by the inclusion of the many-body suppression of neutrino-matter scattering rates may be one of the crucial missing pieces of the supernova puzzle. However, we caution that the actual magnitude and functional form of all the various many-body corrections to the neutrino-matter rates (both neutral- and charged-current), however important they seem from our current simulations, still need to be explored and verified.

We performed a test using the ray-by-ray+ approximation to neutrino transport in a manner similar to that employed by Skinner et al. (2016) to gauge its effect

on the outcome of collapse when a full physics suite is employed. In Skinner et al. (2016), it was shown that ray-by-ray+ artificially enhanced heating along the poles in synchrony with the axial sloshing seen in 2D simulations and thereby made models more explosive. Here, we focused on the  $20\text{-}M_{\odot}$  progenitor of Woosley & Heger (2007) and found that if the model had exploded very late without this approach (using more realistic and truly multi-D transport) that it exploded significantly earlier when the ray-by-ray+ method was employed. This temporal shift can be as large as the full range in explosion times currently witnessed by the various supernova simulation groups for a given progenitor. One can speculate that had groups that use the ray-by-ray+ simplification used real multi-D transport their 2D models would have exploded later, perhaps much later or not at all. Speculating further, one wonders whether, since non-rotating 3D simulations seldom manifest the axial sloshing seen in 2D and may, as a result, be less susceptible to the ray-by-ray+ anomaly, that the fact that 3D models explode later than the corresponding 2D models (Lentz et al. 2015) or not at all (Melson et al. 2015, if without their strangeness fix) may be connected with their use of ray-by-ray+. In short, without ray-by-ray+, it is not clear that 2D would explode much earlier than 3D. However, the differences between the 2D and 3D convective cascades may be equally in play here and the associated simulations still need to be performed to assess this. Nevertheless, we suggest that adding many-body corrections to neutrino-nucleon scattering, which is a real physical effect (even though its magnitude has yet to be definitely pinned down), might in part or wholly compensate for upgrading ray-by-ray+ to full multi-D transport in 3D simulations.

The possible role of initial perturbations as seeds to the growth of convective instability in and around the gain region has been a subject of recent focus. Clearly, allowing grid noise, truncation error, or other numerical noise to initiate linear growth to the non-linear phase, or imposing artificial initial perturbations, is less than satisfactory. This is particularly true given that seeds have a finite time to grow after accreting through the shock before leaving the unstable region and given that the time to instability and explosion is germane to which phase of the neutrino light curve is driving explosion. Inaugurating the non-linear convective phase early and maintaining it until explosion may be important, and the magnitude and timing of convective seeding is therefore of interest. Though we have deferred until later a more comprehensive study of this subject, we tested the effect of adding to the progenitor velocity perturbations whose magnitude was informed by mixing-length theory (Müller et al. 2016). In fact, we allowed the maximum perturbation speed to be  $1000\text{ km s}^{-1}$ , with a Mach number as high as  $\sim 0.12$ , which is a bit larger than found in 1D progenitor models (cf. Woosley & Heger 2007). Indeed, we found that large imposed perturbations of this sort accelerated the time to explosion for an otherwise late explosion. In summary, we did not find such imposed perturbations critical to explosion, but found that they can aide an otherwise marginal one. Nevertheless, it will be important to determine their character, and the many 3D-progenitor studies now in process promise

to do just that.

Many-body corrections to scattering rates, inelastic scattering, and initial seed perturbations all boost “explodability,” increase explosion energy, and shorten the time to explosion. In fact, these effects add synergistically and non-linearly to aide explosion, despite the fact that they individually amount to effects at the  $\sim 10\text{--}30\%$  level. This is due to the proximity of multi-D models to criticality, and is not seen in 1D simulations.

Furthermore, the turbulence behind the shock that has been shown to aid explosion in the realistic multi-D context naturally introduces indeterminacy in detail. Even the same progenitor star, but with different random seed perturbations and rotational structures at collapse, should yield a range of explosion energies, nucleosynthesis,  $^{56}\text{Ni}$  yields, pulsar kicks, and explosion morphologies. Therefore, it is expected that Nature provides distribution functions, and not one-to-one maps, in all signatures of explosion. In the long run, theory will need to come to grips with this, but in the short run one should not expect that in the chaotic context of turbulent convection and pre-collapse structures the best models will correspond in detail. This is the physical and natural consequence of chaos, and will be paralleled in comparison verification studies.

We now find that all our multi-D models with realistic physics explode by the neutrino heating mechanism. Proximity to criticality amplifies the role of even small neutrino-matter effects. In particular, the effect of the many-body structure-factor correction to neutrino-nucleon scattering on the driving  $\nu_e$  and  $\bar{\nu}_e$  luminosities and average energies boosts explodability, as does inelastic scattering off electrons and nucleons. This might offset the negative effect on the results for those using the problematic ray-by-ray+ approach of converting to fully multi-D transport, although this has yet to be determined in 3D. Imposing perturbations of significance is also modestly supportive of explosion, but does not seem necessary.

The next stage is to explore the same issues in three dimensions, and it is only after performing such simulations, and their subsequent verification, that a robust resolution to the core-collapse supernova problem can be claimed. Nevertheless, there has been significant progress of late in unraveling this central mystery in astrophysics, in demonstrating the viability of the

neutrino-driven mechanism of explosion, and in illuminating its component physics. It was with these ultimate goals in mind that this paper was forged.

The authors acknowledge the help of Evan O’Connor with the Lattimer-Swesty equation of state and of Todd Thompson, who was instrumental in developing the inelastic scattering tables and schema. In addition, they thank Chuck Horowitz for early conversations concerning the neutrino response in nuclear matter at low densities, his insights into neutrino-matter interaction physics, and for an advanced look at his recent paper on these topics. Finally, they would like to thank Yukiya Saito and Junichiro Iwasawa for help scrutinizing the various progenitor model sets in the literature and Sean Couch for stimulating conversations on a variety of core-collapse topics. Support was provided by the Max-Planck/Princeton Center (MPPC) for Plasma Physics (NSF PHY-1144374) and the NSF PetaApps program, under award OCI-0905046 via a subaward no. 44592 from Louisiana State University to Princeton University. The authors employed computational resources provided by the TIGRESS high performance computer center at Princeton University, which is jointly supported by the Princeton Institute for Computational Science and Engineering (PICSciE) and the Princeton University Office of Information Technology, and by the National Energy Research Scientific Computing Center (NERSC), which is supported by the Office of Science of the US Department of Energy (DOE) under contract DE-AC03-76SF00098. The authors express their gratitude to Ted Barnes of the DOE Office of Nuclear Physics for facilitating their use of NERSC. This work was originally part of the “Three Dimensional Modeling of Core-Collapse Supernovae” PRAC allocation support by the National Science Foundation (award number ACI-1440032) and was part of the Blue Waters sustained-petascale computing project, which is supported by the National Science Foundation (awards OCI-0725070 and ACI-1238993) and the state of Illinois. Blue Waters is a joint effort of the University of Illinois at Urbana-Champaign and its National Center for Supercomputing Applications. This paper has been assigned a LANL preprint # LA-UR-16-28849.

## APPENDIX

Using FORNAX, we solve the equations of hydrodynamics and lepton number conservation. With neutrino source and sink terms, they are:

$$\rho_{,t} + (\rho v^i)_{;i} = 0, \quad (1)$$

$$(\rho v_j)_{,t} + (\rho v^i v_j + P \delta_j^i)_{;i} = -\rho \phi_{,j} + c^{-1} \sum_s \int_0^\infty (\kappa_{s\varepsilon} + \sigma_{s\varepsilon}^{\text{tr}}) F_{s\varepsilon j} d\varepsilon, \quad (2)$$

$$\left[ \rho \left( e + \frac{1}{2} \|v\|^2 \right) \right]_{,t} + \left[ \rho v^i \left( e + \frac{1}{2} \|v\|^2 + \frac{P}{\rho} \right) \right]_{;i} = -\rho v^i \phi_{,i} \quad (3)$$

$$- \sum_s \int_0^\infty \left( j_{s\varepsilon} - c \kappa_{s\varepsilon} E_{s\varepsilon} - \frac{v^i}{c} (\kappa_{s\varepsilon} + \sigma_{s\varepsilon}^{\text{tr}}) F_{s\varepsilon i} \right) d\varepsilon, \quad (4)$$

$$(\rho Y_e)_{,t} + (\rho Y_e v^i)_{;i} = \sum_s \int_0^\infty \xi_{s\varepsilon} (j_{s\varepsilon} - c \kappa_{s\varepsilon} E_{s\varepsilon}) d\varepsilon, \quad (5)$$

where  $e$  is the specific internal energy,  $P = P(\rho, e, Y_e)$  is the pressure,  $\rho$  is the mass density,  $Y_e$  is the electron fraction,  $v_i$  are the velocity components,  $\kappa_{s\varepsilon}$  and  $\sigma_{s\varepsilon}^{\text{tr}}$  are the absorption and transport scattering opacities, and  $s \in \{\nu_e, \bar{\nu}_e, \nu_x\}$ , where

$$\xi_{s\varepsilon} = \begin{cases} -(N_A \varepsilon)^{-1} & s = \nu_e, \\ (N_A \varepsilon)^{-1} & s = \bar{\nu}_e, \\ 0 & s = \nu_x. \end{cases} \quad (6)$$

The basic equations of radiative transfer in the comoving frame that we solve are the zeroth- and first-moment equations of the full equation of radiative transfer for the specific intensity of the  $\nu_e$ ,  $\bar{\nu}_e$ , and  $\nu_x$  neutrinos, where the latter represents the  $\nu_\mu$ ,  $\bar{\nu}_\mu$ , and  $\nu_\tau$ , neutrinos collectively. The equations, modified to approximately incorporate general relativistic effects, are:

$$E_{s\varepsilon,t} + (\alpha F_{s\varepsilon}^i + \mathbf{v}^i \mathbf{E}_{s\varepsilon})_{;i} - \alpha \mathbf{v}_{;j}^i \frac{\partial}{\partial \ln \varepsilon} \mathbf{P}_{s\varepsilon i}^j = \alpha (j_{s\varepsilon} - c \kappa_{s\varepsilon} E_{s\varepsilon}) + \alpha G^e, \quad (7)$$

$$F_{s\varepsilon j,t} + (c^2 \alpha P_{s\varepsilon j}^i + \mathbf{v}^i \mathbf{F}_{s\varepsilon j})_{;i} + \alpha \mathbf{v}_{;j}^i \mathbf{F}_{s\varepsilon i} - \alpha \mathbf{v}_{;k}^i \frac{\partial}{\partial \varepsilon} (\varepsilon \mathbf{Q}_{s\varepsilon j i}^k) = -c \alpha (\kappa_{s\varepsilon} + \sigma_{s\varepsilon}^{\text{tr}}) F_{s\varepsilon j} + \alpha G_j^m, \quad (8)$$

where differentiation is indicated with standard notation,  $\varepsilon$  is the neutrino energy,  $s \in \{\nu_e, \bar{\nu}_e, \nu_x\}$ ,  $E_{s\varepsilon}$  is the radiation energy density spectrum (zeroth moment),  $F_{s\varepsilon j}$  is radiation flux spectrum (first moment),  $P_{s\varepsilon i}^j$  is the radiation pressure tensor (second moment),  $Q_{s\varepsilon j i}^k$  is the heat tensor (third moment),  $\alpha = \exp(\phi/c^2)$ , and the other variables have their standard meanings.  $\phi$  is the gravitational potential. We use the M1 closure to truncate the radiation moment hierarchy by specifying the second and third moments in terms of the zeroth and first.

$G^e$  and  $G_j^m$  are the main terms to add in order to include gravitational redshifts (Rampp & Janka 2002; Shibata et al. 2011). They are given by

$$G^e = -\mathbf{F}_{s\varepsilon} \cdot \nabla \phi / c^2 + \nabla \phi / c^2 \cdot \partial (\varepsilon \mathbf{F}_{s\varepsilon}) / \partial \varepsilon, \quad (9)$$

$$G_j^m = -E_{s\varepsilon} \nabla_j \phi / c^2 + \nabla_i \phi / c^2 \cdot \partial (\varepsilon \mathbf{P}_{s\varepsilon j}^i) / \partial \varepsilon, \quad (10)$$

where  $\nabla_j \phi / c^2 = -g_j / c^2$ , and one must do the contravariant/covariant raising or lowering according to the metric. Notice that the last terms in the equations for  $G^e$  and  $G_j^m$  integrate out to zero when one integrates over energy groups, leaving the terms analogous to the “ $\rho \mathbf{v} \cdot \mathbf{g}$ ” and “ $\rho \mathbf{g}$ ” work and force terms.

The gravitational potential,  $\phi$ , is generally taken to be the “GR-corrected” monopole term ( $\phi_{\text{TOV}}$ ). There are a variety of ways to approximate this, and the source for this approximation is Marek et al. (2006). Many people use their “Case A,” as do we, though they say their “Case B” is also very good. The relevant equations are:

$$\frac{d\phi_{\text{TOV}}}{dr} = G \frac{m_{\text{TOV}} + 4\pi r^3 (P + P_\nu) / c^2}{r^2 \Gamma^2} \left[ \frac{\rho + E/c^2 + P/c^2}{\rho} \right], \quad (11)$$

$$\Gamma(r) = \sqrt{1 + v^2/c^2 - \frac{2Gm_{\text{TOV}}(r)}{rc^2}}, \quad (12)$$

$$\frac{dm_{\text{TOV}}}{dr} = 4\pi r^2 \left( \rho + E/c^2 + E_\nu/c^2 + \frac{\mathbf{v} \cdot \mathbf{F}_\nu / c^2}{\Gamma} \right) \Gamma \quad (\text{Case A}), \quad (13)$$

$$\frac{dm_{\text{TOV}}}{dr} = 4\pi r^2 \rho \quad (\text{Case B}), \quad (14)$$

where  $\rho$  is the rest mass density,  $P_\nu$  is the total neutrino pressure,  $E$  is the total matter internal energy density,  $P$  is the matter pressure,  $v$  is some averaged radial speed,  $E_\nu$  is the total neutrino energy density, and  $F_\nu$  is the total

neutrino flux. If one is using a multipole expansion to derive the potential, then the potential used is:

$$\phi_{\text{eff}} = \phi - \bar{\phi} + \phi_{\text{TOV}}, \quad (15)$$

where  $\phi$  is the multipole Newtonian potential,  $\bar{\phi}$  is the monopole Newtonian potential, and  $\phi_{\text{TOV}}$  is the monopole TOV potential. Note that this equation merely subtracts out the monopole term from the total Newtonian potential, and then adds it back, corrected for the GR effects in the approximate way suggested by Marek et al. (2006).

So, one needs to calculate the total pressure, energy density, and flux of the neutrinos, calculate  $\langle v^2/c^2 \rangle$  as a function of radius, and then integrate radially/spherically to get  $m_{\text{TOV}}$  and  $\phi_{\text{TOV}}$ . All the non-monopolar potential contributions (if included) are Newtonian; only the monopole term is adjusted approximately for GR. This correction to the monopolar potential used in the matter momentum equation is likely the dominant effect of GR. However, the “GR-corrected” transport scheme above incorporates the neutrino energy redshifts, as well as the time dilation. In the steady state, zero-motion limit, the total luminosity  $\times \exp(2\phi/c^2)$  is a constant, as it should be (note the factor of 2).

## REFERENCES

- Abdikamalov, E., Zhaksylykov, A., Radice, D., & Berdibek, S. 2016, *MNRAS*, 461, 3864 (arXiv:1605.09015)
- Ahmed, Z., et al. 2012, *Phys. Rev. Lett.*, 108, 102001
- Bethe, H. & Wilson, J.R. 1985, *ApJ*, 295, 14
- Brandt, T. D., Burrows, A., Ott, C. D., & Livne, E. 2011, *ApJ*, 728, 8
- Bruenn, S.W. 1985, *ApJS*, 58, 771
- Bruenn, S.W. & Dineva, T. 1996, *ApJ*, 458, L71
- Bruenn, S. W., Mezzacappa, a., Hix, W.R. et al. 2013, *ApJ*, 767, L6
- Bruenn, S.W., Lentz, E.J., Hix, W.R. et al., *ApJ*, 818, 123
- Buras, R., Rampp, M., Janka, H.-T., & Kifonidis, K. 2003, *Phys. Rev. Lett.*, 90, 241101
- Buras, R., Janka, H.-T., Rampp, M., & Kifonidis, K. 2006, *A&A*, 457, 281
- Burrows, A. & Lattimer, J.M. 1983, *ApJ*, 270, 735
- Burrows, A., & Goshy, J. 1993, *ApJ*, 416, L75
- Burrows, A., Hayes, J., & Fryxell, B.A. 1995, *ApJ*, 450, 830
- Burrows, A. & Sawyer, R.F. 1998, *Phys. Rev. C*, 58, 554
- Burrows, A. & Sawyer, R. 1999, *Phys. Rev. C*, 59, 510
- Burrows, A. 2004, “Core-Collapse Supernova Theory, Rotation, and Quasi-Bipolar Explosions,” in the proceedings of the International Conference “1604-2004: Supernovae As Cosmological Lighthouses,” held at Padua, Italy on 16-19 June, 2004 (ASP Conference Proceedings, V. 342), p. 184
- Burrows, A., Reddy, S., & Thompson, T.A. 2006, *Nuclear Physics A*, 777, 356-394
- Burrows, A., Livne, E., Dessart, L., Ott, C. D., & Murphy, J. 2006, *ApJ*, 640, 878
- Burrows, A., Dessart, L., Livne, E., Ott, C.D., & Murphy, J. 2007a, *ApJ*, 655, 416
- Burrows, A., Dessart, L., & Livne, E. 2007b “The Multi-Dimensional Character and Mechanisms of Core-Collapse Supernovae,” in the proceedings of the conference “SUPERNOVA 1987A: 20 YEARS AFTER; Supernovae and Gamma-Ray Bursters,” (AIP Proceedings Series), V. 937, pp. 370-380, held in Aspen, CO, February 19-23.
- Burrows, A., Dessart, L., Livne, E., Ott, C.D. & Murphy, J.W. 2007c, *ApJ*, 664, 416
- Burrows, A., Dolence, J. C., & Murphy, J.W. 2012, *ApJ*, 759, 5
- Burrows, A. 2013, *Reviews of Modern Physics*, 85, 245
- Chatzopoulos, E., Couch, S.M., Arnett, W.D., & Timmes, F.X. 2016, *ApJ*, 822, 61
- Chugai, N.N. & Utrobin, V.P. 2014, *Astronomy Letters*, 40, 291
- Couch, S.M., & Ott, C.D. 2013, *ApJ*, 778, L7
- Couch, S.M., & Ott, C.D. 2015, *ApJ*, 799, 5, 2015 (arXiv:1408.1399)
- Couch, S.M., Chatzopoulos, E., Arnett, W.D., & Timmes, F. 2015, arXiv:1503.02199
- Dessart, L., Burrows, A., Livne, E., & Ott, C. D. 2006, *ApJ*, 645, 534
- Dolence, J. C., Burrows, A., Murphy, J. W., & Nordhaus, J. 2013, *ApJ*, 765, 110
- Dolence, J., Burrows, A., & Zhang, W. 2015, *ApJ*, 800, 10 (arXiv:1403.6115)
- Dolence, J., Burrows, A. & Skinner, M.A. 2016, to be submitted to *ApJS*
- Dubroca, B., & Feugeas, J.L. 1999, *CRAS*, 329, 915
- Emmering, R.T., & Chevalier, R.A. 1989, *ApJ*, 345, 931
- Eriguchi, Y., Müller, E. 1984, *A&A*, 147, 16
- Ertl, T., Janka, H.-Th., Woosley, S.E., Sukhbold, T., & Ugliano, M. 2015, arXiv:1503.07522
- Faucher-Giguere C.-A., Kaspi V. 2006, *ApJ*, 643, 355
- Fischer, T. 2016, submitted to *Phys. Rev. C*, arXiv:1608.05004
- Fryer, C.L. & Heger, A. 2000, *ApJ*, 541, 1033
- Hanke, F., Marek, A., Müller, & Janka, H.-T. 2012, *ApJ*, 770, 66
- Hanke, F., Müller, B., Wongwathanarat, A., Marek, A., & Janka, H.-T. 2013, *ApJ*, 770, 66
- Hannestad, s. & Raffelt, G. 1998, *ApJ*, 507, 339
- Heger, A., Woosley, S.E., Langer, N., & Spruit, H.C. 2003, “Presupernova Evolution of Rotating Massive Stars and the Rotation Rate of Pulsars,” in “Stellar Rotation,” published in the proceedings of the IAU Symposium No. 215, eds. A. Maeder & P. Eeneens (International Astronomical Union)
- Horowitz, C.J. 2002, *Phys. Rev. D*, 65, 043001
- Horowitz, C.J., Caballero, O.L., Lin, Z., O’Connor, E., & Schwenk, A. 2016, submitted to *Phys. Rev. C*(arXiv:1611.05140)
- Iwakami, W., Nagakura, H., & Yamada, S. 2014, *ApJ*, 793, 5 (arXiv:1404.2646)
- Kitaura, F.S., Janka, H.-T., & Hillebrandt, W. 2006, *A&A*, 450, 345
- Kurtz, D.W., Saio, H., Masao, T., Shibahashi, H., Murphy, S.J., & Sekii, T. 2014, accepted to *MNRAS*(arXiv:1405.0155)
- Janka, H.-T., & Müller, E. 1996, *A&A*, 306, 167
- Janka, H.-T., Keil, W., Raffelt, G., & Seckel, D. 1996, *Phys. Rev. Lett.*, 76, 2621
- Janka, H.-T. 2012, *Annual Review of Nuclear and Particle Science*, 62, 407
- Just, O., Obergaulinger, M., & Janka, H.-T. 2015, *MNRAS*, 453, 3386 (arXiv:1501.0299)
- Lattimer, J.M., & Swesty, F. D. 1991, *Nucl. Phys.*, A535, 331
- Lentz, E.J., Bruenn, S.W., Hix, W.R., Mezzacappa, A., Messer, O.E.B., Endeve, E., Blondin, J.M., Harris, J.A., Marronetti, P., & Yakunin, K.N. 2015, *ApJ*, 807, 31 (arXiv:1505.05110)
- Liebrandt, M., Whitehouse, S. C., & Fischer, T. 2009, *ApJ*, 698, 1174
- MacFadyen, A.I. & Woosley, S.E. 1999, *ApJ*, 524, 262
- Marek, A., Dimmelmeier, H., Janka, H.-T., Müller, E., & Buras, R. 2006, *A&A*, 445, 273
- Marek, A., & Janka, H.-T. 2009, *ApJ*, 694, 664
- Meakin, C. A., Sukhbold, T., & Arnett, W. D. 2011, *Ap&SS*, 336, 123
- Melson, T., Janka, H.-T., Bollig, R., et al. 2015, *ApJ*, 808, 42 (arXiv:1504.07631)
- Mezzacappa, A. & Bruenn, S.W. 1993, *ApJ*, 405, 637
- Müller, E., & Steinmetz, M. 1995, *Computer Physics Communications*, 89, pp. 45-58
- Müller, B., Janka, H.-T., & Dimmelmeier, H. 2010, *ApJS*, 189, 104
- Müller, B., Janka, H.-T., & Heger, A. 2012a, *ApJ*, 761, 72
- Müller, B., Janka, H.-T., & Marek, A. 2012b, *ApJ*, 756, 84
- Müller, B. & Janka, H.-T. 2015, *MNRAS*, 448, 2141, arXiv:1409.4783
- Müller, B., Viallet, M., Heger, A., & Janka, H.-T. 2016, arXiv:1605.01393
- Müller, B. 2016, *Publs. Astron. Soc. of Aust. (PASA)*, 33, id.e048 (arXiv:1608.03274)
- Murphy, J. W., & Burrows, A. 2008, *ApJ*, 688, 1159

- Murphy, J. W., Dolence, J. C., & Burrows, A. 2013, *ApJ*, 771, 52
- Nakamura, K., Kuroda, T., Takiwaki, T., & Kotake, K. 2014, *ApJ*, 793, 45 (arXiv:1403.7290)
- Nomoto, K. & Hashimoto, M. 1988, *Physics Reports*, 163, 13
- Noutsos A., Schnitzler D.H.F.M., Keane E.F., Kramer M., & Johnston S., 2013, *MNRAS*, 430, 2281
- Abdikamalov, E., Zhaksylykov, A., Radice, D., & Berdibek, S. 2016, *MNRAS*, 461, 3864
- O'Connor, E. & Ott, C.D. 2011, *ApJ*, 730, 70
- O'Connor, E. & Ott, C.D. 2013, *ApJ*, 762, 126
- O'Connor, E. & Couch, S. 2015, submitted to *ApJ*(arXiv:1511.07443)
- Ott, C. D., Burrows, A., Dessart, L., & Livne, E. 2008, *ApJ*, 685, 1069
- Popov, S.B. & Turolla, R. 2012, *Ap&SS*, 341, 457
- M. Rampp, M. & Janka, H.-T. 2002, *A&A*, 396, 361
- Reddy, S., Prakash, M., Lattimer, J.M., & Pons, J.A. 1999, *Phys. Rev. C*, 59, 2888
- Roberts, L.F., Reddy, S., & Shen, G. 2012, *Phys. Rev. C*, 86, 065803 (arXiv:1205.4066)
- Shibata, M., Kiuchi, K., Sekiguchi, Y., & Suwa, Y. 2011, *Progress of Theoretical Physics*, 125, 1255
- Skinner, M.A., Burrows, A., & Dolence, J. 2016, accepted to *ApJ*(arXiv:1512.00113)
- Sukhbold, T. & Woosley, S.E. 2014, *ApJ*, 783, 10
- Sukhbold, T., Ertl, T., Woosley, S.E., Brown, J.M., & Janka, H.-T. 2015, *ApJ*, 821, 38
- Sumiyoshi, K., Takiwaki, T., Matsufuru, H. & Yamada, S. 2015, *ApJS*, 216, 37 (arXiv:1403.4476)
- Summa, A., Hanke, F., Janka, H.-T., Melson, T., Marek, A., & Müller, B. 2016, *ApJ*, 825, 6 (arXiv:1511.07871)
- Suwa, Y., Kotake, K., Takiwaki, T., Whitehouse, S. C., Liebendörfer, M., & Sato, K. 2010, *PASJ*, 62, L49
- Takiwaki, T., Kotake, K., & Suwa, Y. 2012, *ApJ*, 749, 98 (arXiv:1108.3989)
- Takiwaki, T., Kotake, K., & Suwa, Y. 2016, *MNRAS*, 461, L112 (arXiv:1602.06759)
- Tamborra, I., Hanke, F., Janka, H.-T., Mueller, B., Raffelt, G. G., & Marek, A. 2014, arXiv:1402.5418
- Thompson, T.A., Burrows, A., & Horvath, J.E. 2000, *Phys. Rev. C*, 62, 035802
- Thompson, T.A., Burrows, A., & Pinto, P. 2003, *ApJ*, 592, 434
- Tubbs, D.L. 1979, *ApJ*, 231, 846
- Vaytet, N.M.H., Audit, E., Dubroca, B., & Delahaye, F. 2011, *JQSRT*, 112, 1323
- Wheeler, J.C., Kagan, D., & Chatzopoulos, E. 2014, *ApJ*, 799, 85 (arXiv:1411.5714)
- Woosley, S. E., & Heger, A. 2007, *Phys. Rep.*, 442, 269
- Zhang, W., Howell, L., Almgren, A., Burrows, A., & Bell, J. 2011, *ApJS*, 196, 20
- Zhang, W., Howell, L., Almgren, A., Burrows, A., Dolence, J., & Bell, J. 2013, *ApJS*, 204, 7

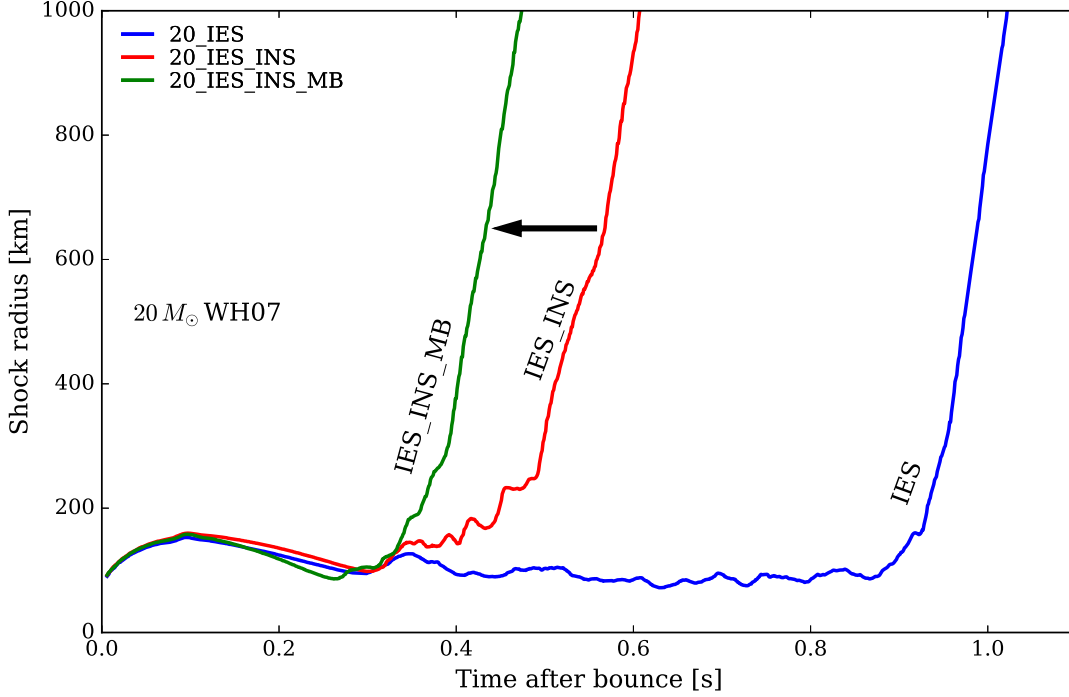


FIG. 1.— Here, we plot the mean shock radii (in kilometers) for our 2D simulations of the 20- $M_{\odot}$  progenitor from Woosley & Heger (2007) as a function of time (in seconds) after bounce. The addition of inelastic scattering off nucleons (IES\_INS, in red) accelerates the explosion time relative to a model with only inelastic scattering off electrons (IES, blue). Relative to the IES\_INS model, that with the many-body correction (IES\_INS\_MB, green) accelerates it even further. The difference in the explosion time between the IES and the IES\_INS\_MB models is  $\sim 700$  milliseconds. In all subsequent figures, the IES\_INS\_MB mean shock radii are included in green as a benchmark. See text in §3 for a discussion.

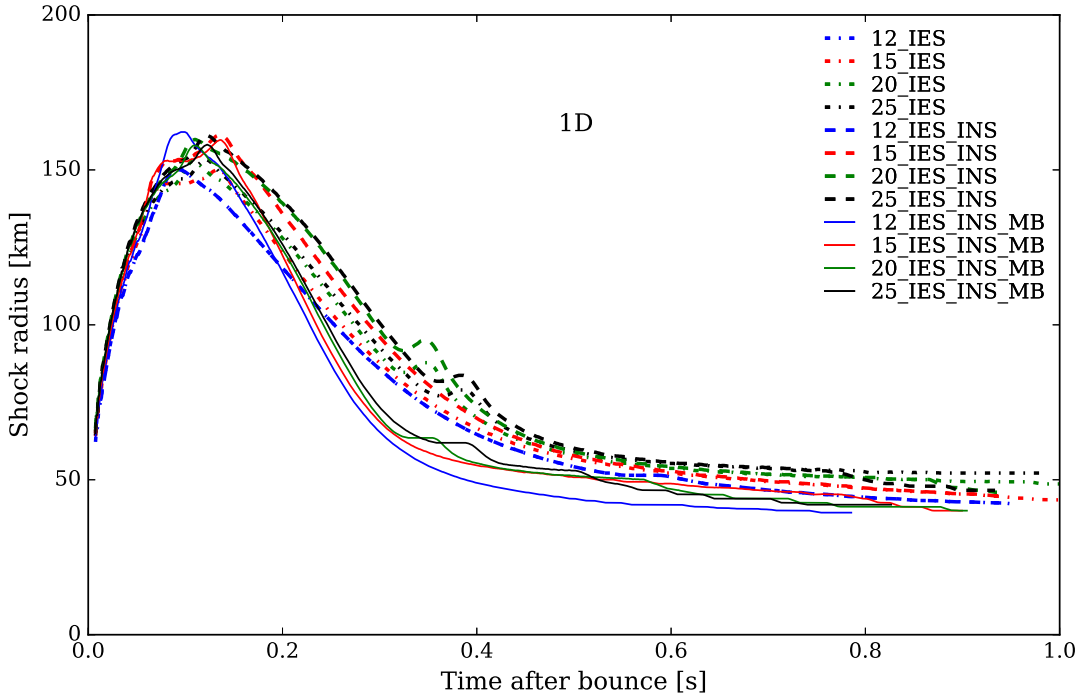


FIG. 2.— The mean shock radii for 1D simulations of the Woosley & Heger (2007) progenitor mass sequence 12 (blue), 15 (red), 20 (green), and 25 (black)  $M_{\odot}$ . Shown are models with only inelastic scattering off electrons (IES, dot-dashed), inelastic scattering off both electrons and nucleons (IES\_INS, dashed), and adding the many-body effect on top (IES\_INS\_MB, solid). None of these 12 models explodes in 1D.

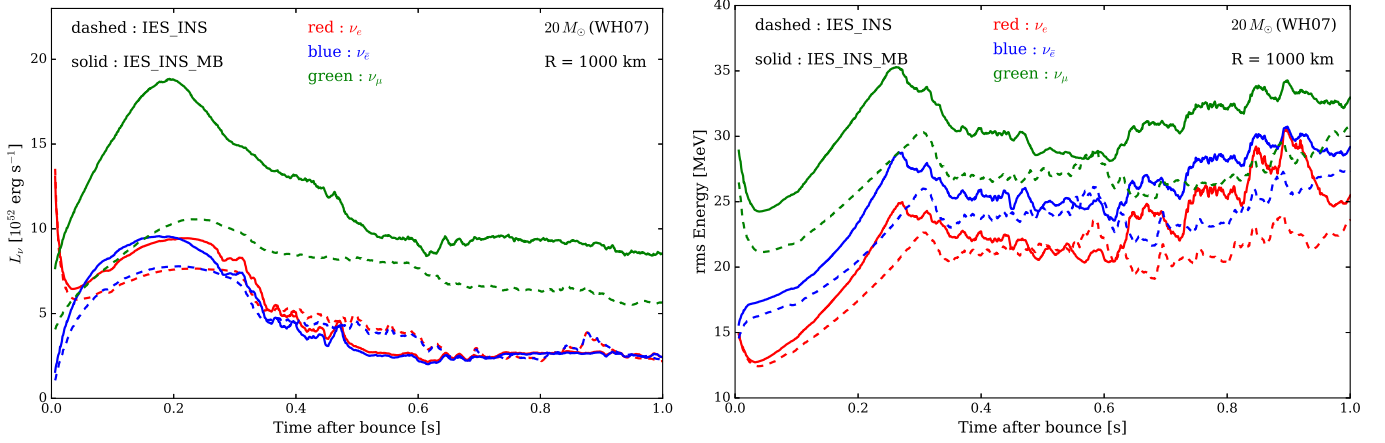


FIG. 3.— The evolution of the mean neutrino luminosities at 1000 km (left, in units of  $10^{52} \text{ erg s}^{-1}$ ) and rms energies (right, in units of MeV) for the  $20 M_\odot$  of Woosley & Heger (2007), illustrating the effect of the many-body (MB) correction (solid lines) on models with inelastic scattering off both electrons and nucleons (dashed lines). With the inclusion of the MB correction, the  $\nu_e$  and  $\bar{\nu}_e$  luminosities increase, but the most significant effect is the increase in the  $\nu_\mu$  luminosities. This leads to increased core compactness and, hence, increased inner core temperatures and the consequent boost in  $\nu_e$  and  $\bar{\nu}_e$  luminosities and neutrino energies seen. As illustrated in Fig. 1, this favors an earlier explosion. The dip in luminosities and rms energies shortly after  $\sim 300$  milliseconds in the MB models corresponds to explosion. See text in §3 for a discussion.

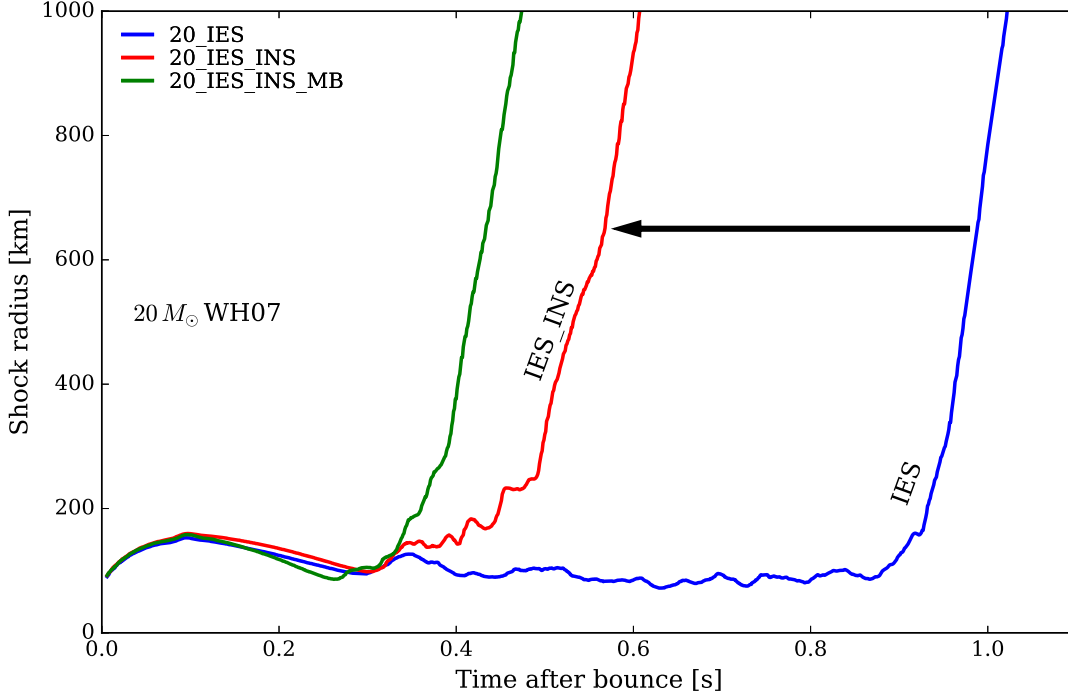


FIG. 4.— Similar to Fig. 1, but now we highlight the effect of including inelastic scattering off nucleons (IES\_INS, red) as well as electrons to a model with only the latter (IES, blue). Plotted for reference is also the benchmark with many-body corrections as well (IES\_INS\_MB, green). Inclusion of INS accelerates explosion of the  $20 M_\odot$  model by  $\sim 400 \text{ ms}$ .



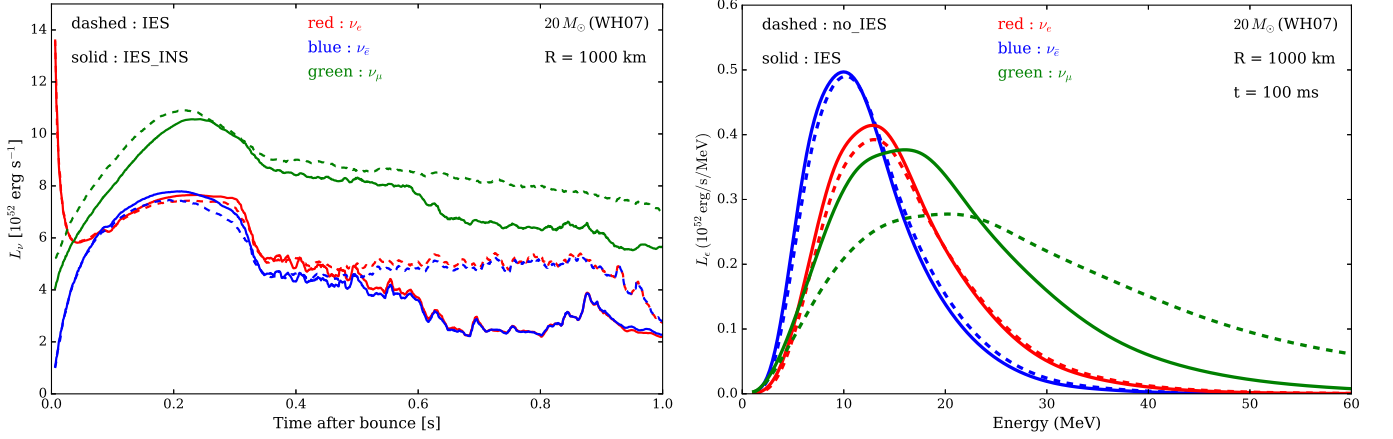


FIG. 5.— Here (on left), we illustrate the effect on the emergent luminosities in the comoving frame of including inelastic scattering off nucleons (solid lines) to a model with inelastic scattering off only electrons (dashed lines). Including inelastic scattering off nucleons, the  $\nu_\mu$  luminosities decrease by roughly 10%, in agreement with Müller et al. (2012b), and the  $\nu_e$ ,  $\bar{\nu}_e$  luminosities increase slightly. The latter effect promotes an earlier explosion. The dip in luminosities shortly after  $\sim 500$  milliseconds corresponds to the explosion of this  $20\text{-}M_\odot$  model. On the right is a plot demonstrating the effect of the inclusion of only inelastic scattering on electrons on the emergent spectrum 100 ms after bounce for the same progenitor. Generally, as has been demonstrated many times in the past, the higher-energy neutrinos are downscattered and the lower-energy neutrinos are upscattered. The effect on the  $\nu_\mu$  neutrinos is the largest.

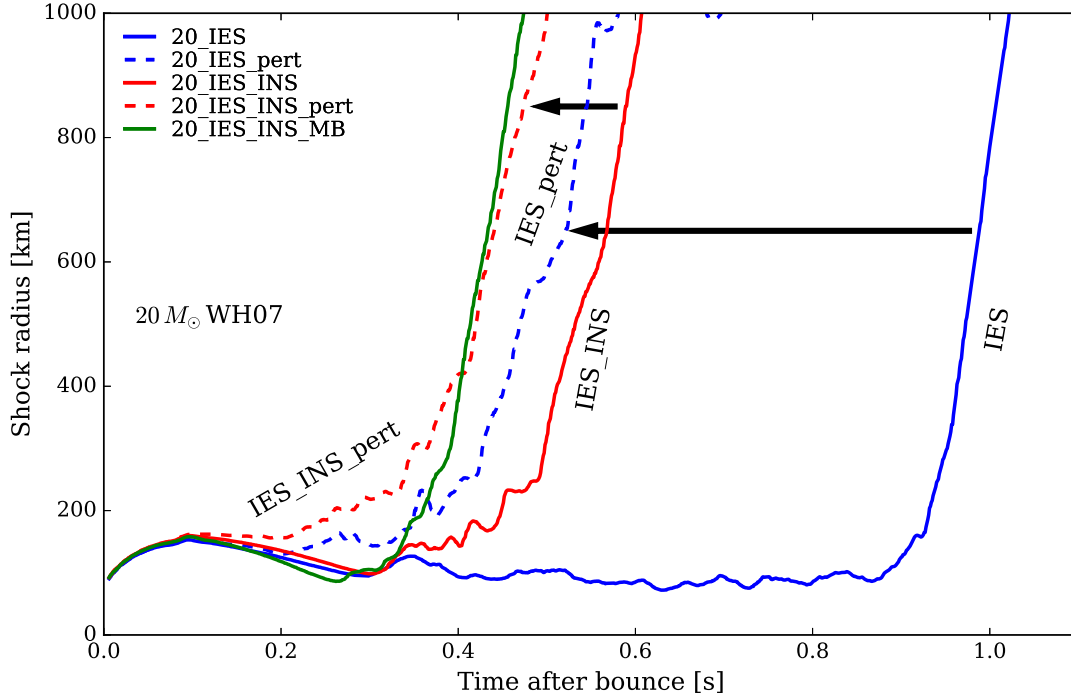


FIG. 6.— Similar to Fig. 1, but illustrating the effect of including velocity perturbations (dashed) for the IES and IES\_INS models (solid). We follow the prescription of Müller & Janka (2015), using a spherical harmonic index  $\ell$  of 2 and a radial quantum number  $n$  of 5 with a maximum velocity perturbation of  $1000\text{ km s}^{-1}$ . Relative to the IES model, including vigorous perturbations accelerates explosion significantly, and including inelastic scattering off nucleons even more. See text in §5 for a discussion.

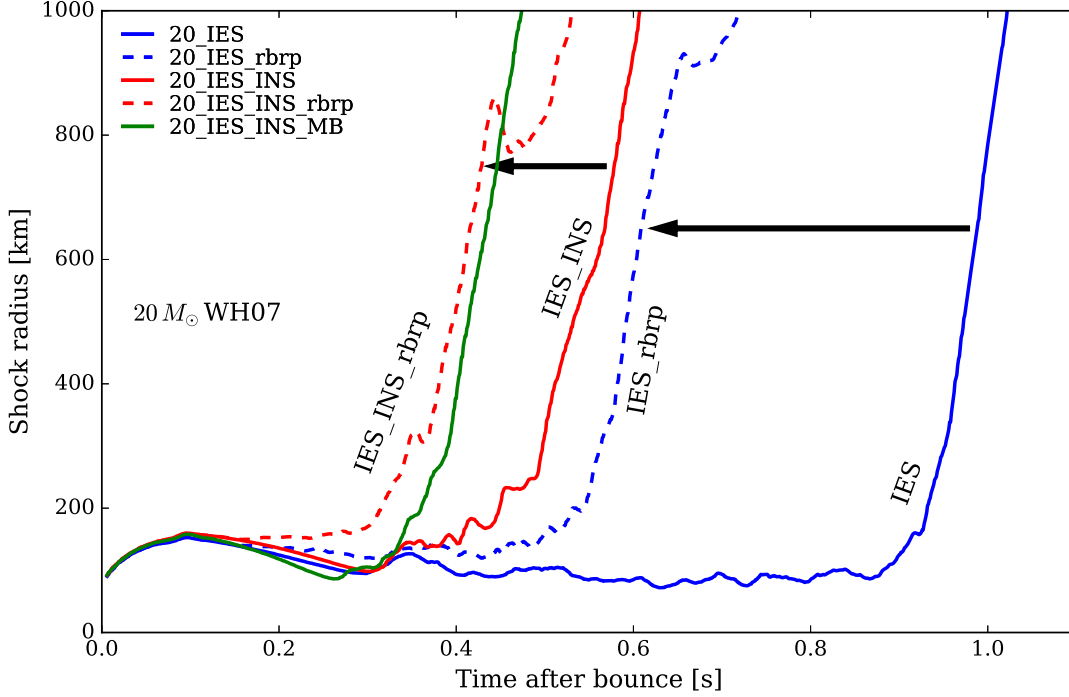


FIG. 7.— Similar to Fig. 1, but illustrating the effect of the use of the ray-by-ray+ approach to neutrino transport (dashed), rather than full multi-D approach (solid). We see that here that the ray-by-ray+ approach can accelerate explosion by  $\sim 500$  ms for the IES (blue) model and by  $\sim 200$  ms for IES\_INS (red) model. See text in §6 for a discussion.

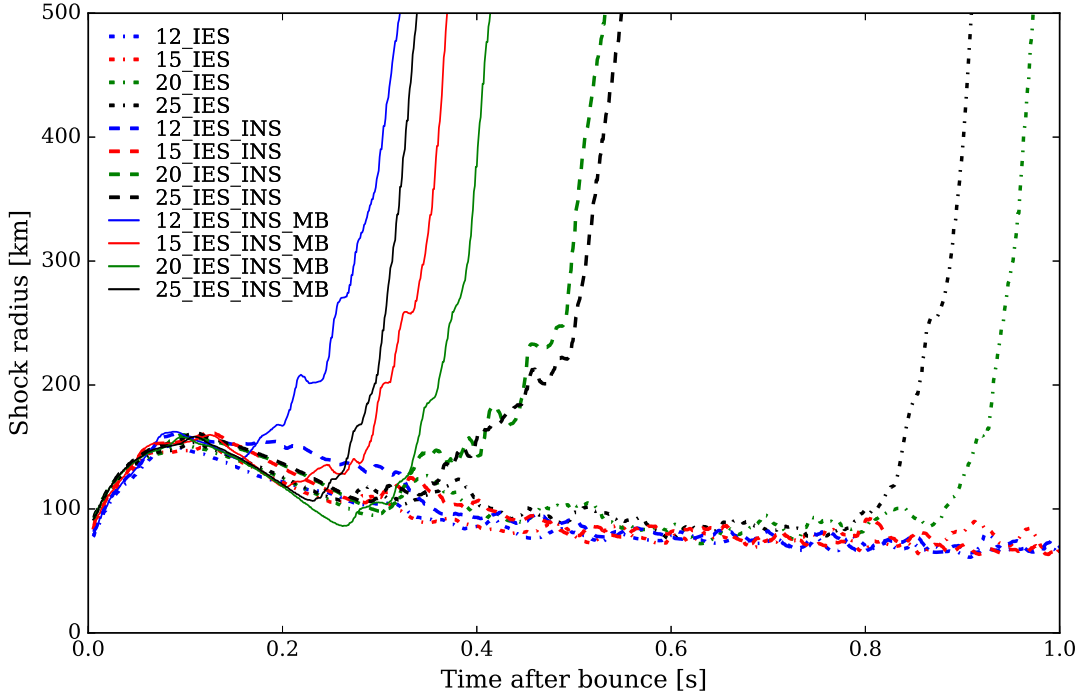


FIG. 8.— Similar to Fig. 2, illustrating three sequences (IES, dot-dashed; IES\_INS, dashed; IES\_INS\_MB, solid) for the same four progenitor masses, but now in 2D. The IES\_INS\_MB models are our benchmark 2D models. The 12- and 15- $M_{\odot}$  models (blue and red lines, respectively) explode within 1.0 second of bounce only with the MB correction, and not with IES or IES\_INS alone. However, with the MB correction, they are the earliest to explode, illustrating the fact that the addition of physical processes can alter the explosion time sequence for the different progenitors. See §7 for a discussion.

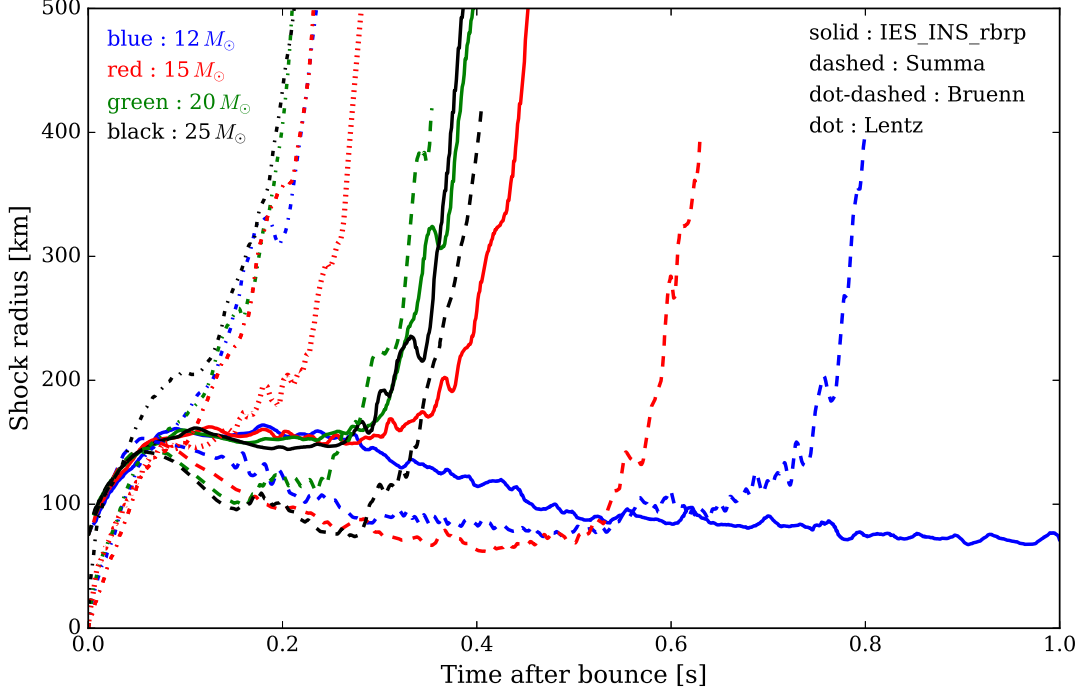


FIG. 9.— Here, for the Woosley & Heger (2007) sequence of four progenitor masses, we compare the shock radius temporal evolutions employing ray-by-ray+ (IES\_INS\_rbrp, solid) with those by Summa et. al (2016) (dashed), with the Series B (dot-dashed) models of Bruenn et. al. (2013,2016), and with the Series C (dot) 15- $M_{\odot}$  model of Lentz et al. (2015). The explosion times of our ray-by-ray+ models and those of Summa et. al. (2016) coincide reasonably well, except for the 12- $M_{\odot}$  progenitor, which did not explode within 1.2 seconds of bounce in our ray-by-ray+ calculation (solid blue). In addition, our ray-by-ray+ simulations achieve larger shock radii in the first several hundred milliseconds post-bounce than those of Summa et al. (2016). The Bruenn et al. (2016) Series B models explode systematically earlier than our ray-by-ray+ models and the Summa et al. (2016) models. The Series C 15- $M_{\odot}$  model explodes slightly later than the Series B model, but still earlier than the other models displayed in this figure. See text in §7 for a discussion.

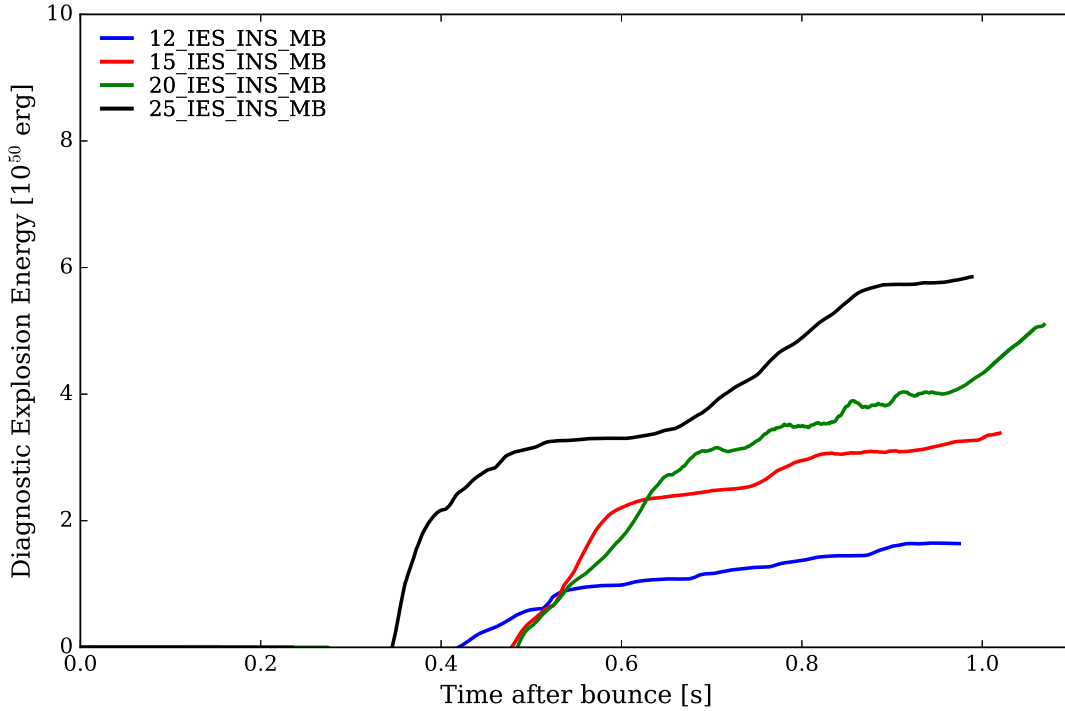


FIG. 10.— The diagnostic explosion energies (in units of Bethes) for six of our exploding models evolved until  $\sim 1.0$  second after bounce (or until the shock reached the edge of the grid at 10,000 km). All four benchmark models with the many-body correction (MB) explode, but only the 20- and 25- $M_{\odot}$  IES\_INS models explode without the MB. The diagnostic energy is calculated using the method of Müller et. al. (2012a) and includes the gravitational potential, kinetic, and internal energies integrated from the radius at which the diagnostic energy becomes positive to the grid edge. See text in §7 for a discussion.

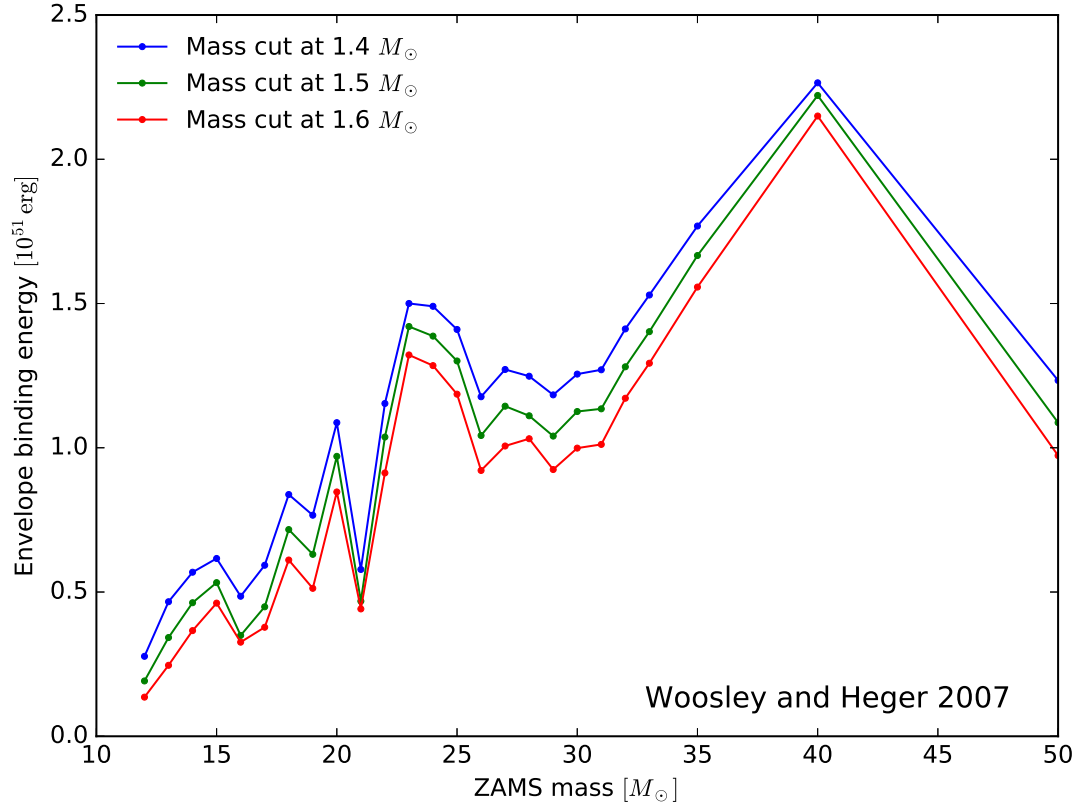


FIG. 11.— The outer envelope binding energies (in Bethes  $\equiv 10^{51}$  erg) for baryon mass cuts of  $1.4$ ,  $1.5$ , and  $1.6 M_{\odot}$  versus ZAMS mass (in  $M_{\odot}$ ) for the Woosley & Heger (2007) progenitor models. See text in §7 for a discussion.

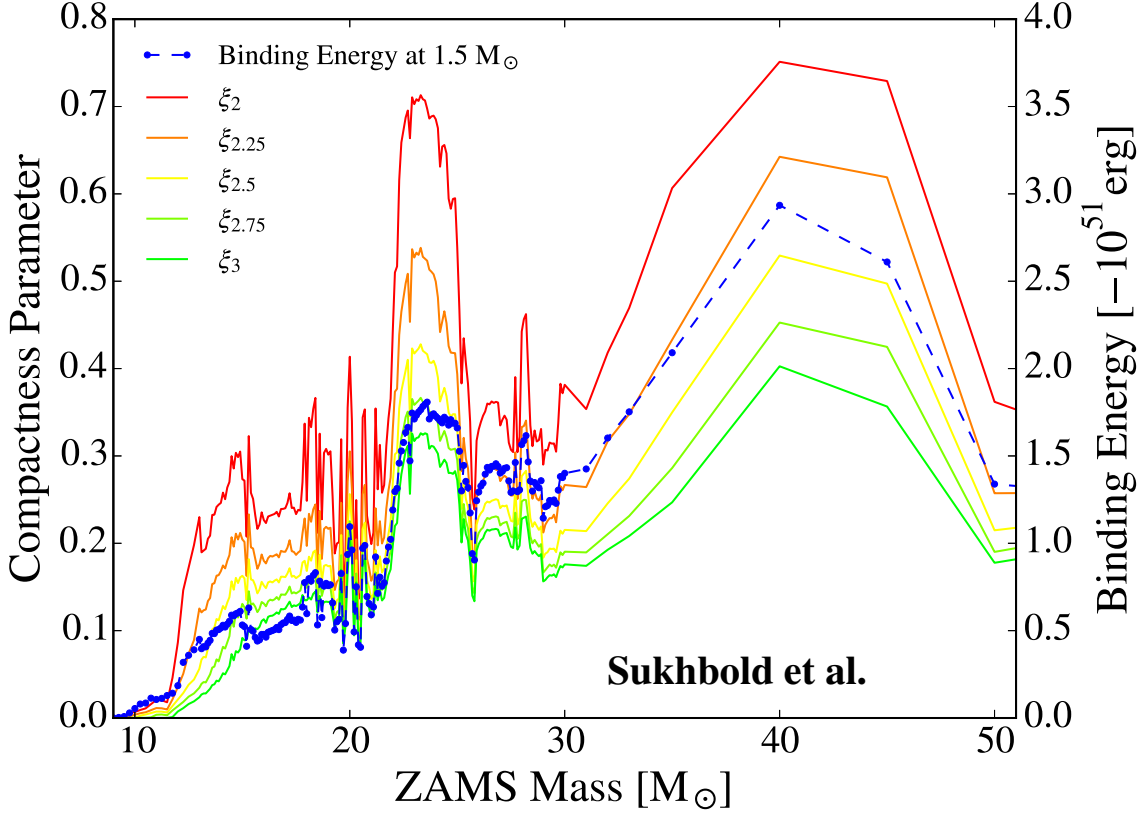


FIG. 12.— This plot depicts the dependence of the compactness parameter (O’Connor & Ott 2011,2013), calculated at various interior masses, versus progenitor ZAMS mass, as well as the corresponding envelope binding energy (blue dots; in Bethes [ $10^{51}$  ergs]) for a baryon mass cut of  $1.5 M_{\odot}$  (see Figure 11). The progenitor models of Sukhbold & Woosley (2014) (also in Sukhbold et al. 2016) are used. As this figure shows, whatever the position at which compactness is defined, it correlates extremely well with envelope binding energy. It is our contention that it is the latter quantity that is more germane to the outcome of core collapse.